

UNIVERSITY OF THESSALY
POLYTECHNIC SCHOOL
DEPARTMENT OF MECHANICAL ENGINEERING

Postgraduate Thesis

**INTRODUCTORY STUDY OF APPLYING PARTICLE-IN-CELL
METHODS IN DETERMINISTIC RAREFIED GAS FLOW
SIMULATIONS**

by
GEORGIOS TATSIOS

Submitted for the Partial Fulfillment
of the Requirements for the Degree of
Master of science

2015

© 2015 Tatsios Georgios

The approval of the Postgraduate Thesis by the Department of Mechanical Engineering of the University of Thessaly does not imply acceptance of the author's opinions.
(Law 5343/32, article 202, paragraph 2).

Εγκρίθηκε από τα Μέλη της Τριμελούς Εξεταστικής Επιτροπής:

Πρώτος Εξεταστής (Επιβλέπων)	Βαλουγεώργης Δημήτριος Καθηγητής, Τμήμα Μηχανολόγων Μηχανικών, Πανεπιστήμιο Θεσσαλίας
Δεύτερος Εξεταστής	Μποντόζογλου Βασίλειος Καθηγητής, Τμήμα Μηχανολόγων Μηχανικών, Πανεπιστήμιο Θεσσαλίας
Τρίτος Εξεταστής	Πελεκάσης Νικόλαος Καθηγητής, Τμήμα Μηχανολόγων Μηχανικών, Πανεπιστήμιο Θεσσαλίας

Certified by the member of the Thesis Committee:

1 st member (Supervisor)	Valougeorgis Dimitrios Professor, Department of Mechanical Engineering, University of Thessaly
2 nd member	Bontozoglou Vasileios Professor, Department of Mechanical Engineering, University of Thessaly
3 rd member	Pelekasis Nikolaos Professor, Department of Mechanical Engineering, University of Thessaly

Acknowledgements

First and foremost, would like to express my gratitude to my supervisor Prof. Dimitris Valougeorgis for all the support and guidance he provided me. Without his teaching, constant inspiration and understanding the research done so far would have not been possible.

I would like to thank the members of the committee, Prof. Vasilios Bontozoglou and Prof. Nikolaos Pelekasis for dedicating their time to read the thesis. I am grateful to my colleagues Christos Tantos, Stergios Naris and Yannis Lyhnaropoulos for the excellent collaboration and interesting discussions.

I would also like to thank my parents, Athanasios and Maria as well as my sister Natasa for their continuous support. Finally, I am especially grateful to Anna Papageorgiou, for her patience and moral support all this time.

Part of this work has been carried out within the framework of the EUROfusion Consortium and has received funding from the Euratom research and training programme 2014-2018 under grant agreement No 633053. The views and opinions expressed herein do not necessarily reflect those of the European Commission.

INTRODUCTORY STUDY OF APPLYING PARTICLE-IN-CELL METHODS IN DETERMINISTIC RAREFIED GAS FLOW SIMULATIONS

Georgios Tatsios

University of Thessaly, Department of Mechanical Engineering, 2015

Supervisor: Valougeorgis Dimitrios, Professor, Department of Mechanical Engineering,
University of Thessaly

Abstract

The field of rarefied gas flow modeling is a gradually growing field of engineering. This is due to the scientific need for accurate results in the fields of vacuum technology, processes and pumping, high altitude aeronautics, space applications and gaseous micro/nano-electromechanical systems. Due to the nature of these flows, typical CFD models based on the Navier-Stokes-Fourier approach are not suitable, and a kinetic approach based on the Boltzmann equation has to be introduced.

Currently two are the leading approaches based purely on kinetic theory, the deterministic solution of the Boltzmann equation using the appropriate kinetic models and the stochastic flow simulation using the Direct Simulation Monte Carlo method (DSMC). Although the deterministic approaches offer great accuracy they are hard to implement in complex geometries or for complicated cases and therefore a very big part of large scale simulations for technological applications is performed using the DSMC method.

In the past, particle-in-cell (PIC) methods have been used to obtain computational results for problems where the typical numerical schemes had proved ineffective. Such methods are relatively easy to implement in complex geometries and owing to their imitative nature complicated particle interaction can be modeled in a straightforward manner.

The present work is an introductory study for the application of particle-in-cell methods for the deterministic simulation of rarefied gas flows. The main steps towards such codes are described and the algorithms for simple cases are formulated. The developed algorithms are benchmarked, using prototype nonlinear problems in plane geometry namely a) the compressible Couette flow, b) the Fourier flow and c) the Poiseuille flow. In all cases very good agreement with published results is achieved, validating the implemented particle-in-

cell methodology and programming codes. This study is a first step towards deterministic particle-in-cell modeling in rarefied gas flows. The potential establishment of PIC methods for deterministically solving such flows is demonstrated.

ΕΙΣΑΓΩΓΙΚΗ ΜΕΛΕΤΗ ΕΦΑΡΜΟΓΗΣ PARTICLE-IN-CELL ΜΕΘΟΔΩΝ ΣΤΗ ΝΤΕΤΕΡΜΙΝΙΣΤΙΚΗ ΠΡΟΣΟΜΟΙΩΣΗ ΑΡΑΙΟΠΟΙΗΜΕΝΩΝ ΡΟΩΝ

Γεώργιος Τάτσιος

Πανεπιστήμιο Θεσσαλίας, Τμήμα Μηχανολόγων Μηχανικών, 2015

Επιβλέπων: Βαλουγεώργης Δημήτριος, Καθηγητής, Τμήμα Μηχανολόγων Μηχανικών,
Πανεπιστήμιο Θεσσαλίας

Περίληψη

Η προσομοίωση αραιοποιημένων ροών αποτελεί ένα αναπτυσσόμενο αντικείμενο της μηχανικής. Το κίνητρο είναι η ανάγκη για ακριβή αποτελέσματα σε περιοχές όπως η τεχνολογία κενού, διαστημική και αεροναυπηγική σε μεγάλα υψόμετρα και ροές αερίων σε μικρο/νάνο-ηλεκτρομηχανολογικά συστήματα και συσκευές. Λόγω της φυσικής που διέπουν αυτές τις περιοχές, τα τυπικά μοντέλα της υπολογιστικής μηχανικής των ρευστών που βασίζονται στην προσέγγιση Navier-Stokes-Fourier δεν είναι κατάλληλα, και κινητικές προσεγγίσεις με βάση την εξίσωση Boltzmann πρέπει να χρησιμοποιηθούν.

Δύο είναι οι κυρίαρχες μέθοδοι επίλυσης βασισμένες στην κινητική θεωρία, η ντετερμινιστική επίλυση της εξίσωσης Boltzmann χρησιμοποιώντας κάποιο κινητικό μοντέλο και η στοχαστική προσομοίωση με τη μέθοδο Direct Simulation Monte Carlo (DSMC). Παρόλο που οι ντετερμινιστικές μέθοδοι προσφέρουν καλύτερη ακρίβεια, είναι προβληματική η εφαρμογή τους σε πολύπλοκες γεωμετρίες ή σε περιπτώσεις σύνθετων ροών, έτσι ένα πολύ μεγάλο τμήμα των προσομοιώσεων μηχανολογικού εξοπλισμού γίνεται με τη μέθοδο DSMC.

Στη βιβλιογραφία, πολλές φορές σωματιδιακές μέθοδοι (Particle-in-Cell) έχουν χρησιμοποιηθεί για την υπολογιστική μελέτη προβλημάτων στα οποία οι συνήθεις αριθμητικές μέθοδοι αποδείχθηκαν ανεπαρκείς. Τέτοιες σωματιδιακές μέθοδοι είναι σχετικά εύκολο να εφαρμοστούν σε πολύπλοκες γεωμετρίες και λόγω του μιμητικού χαρακτήρα τους είναι εύκολο να μοντελοποιήσουν πολύπλοκα φυσικά φαινόμενα.

Στην παρούσα εργασία γίνεται μία εισαγωγική μελέτη της εφαρμογής ντετερμινιστικών σωματιδιακών μεθόδων σε περιπτώσεις αραιοποιημένης ροής. Τα κύρια στάδια της επίλυσης περιγράφονται και γίνεται η μορφοποίηση κάποιων αλγορίθμων για απλές περιπτώσεις. Οι

αλγόριθμοί αυτοί ελέγχονται ως προς την ακρίβεια σε τρία προβλήματα αναφοράς. Συγκεκριμένα εξετάζονται τα μη γραμμικά προβλήματα της συμπιεστής ροής Couette, της μεταφοράς θερμότητας ανάμεσα σε πλάκες (ροή Fourier) και της ροής Poiseuille. Τα αποτελέσματα είναι σε πολύ καλή συμφωνία με αντίστοιχα της βιβλιογραφίας που προέκυψαν με άλλες μεθόδους. Με τον τρόπο αυτό αποδεικνύεται η ορθότητα της προτεινόμενης Particle-in-Cell μεθοδολογίας και των κωδίκων που έχουν αναπτυχθεί στο πλαίσιο της μεταπτυχιακής εργασίας. Αυτή η εργασία αποτελεί ένα αρχικό βήμα στην ντετερμινιστική επίλυση αυτών των προβλημάτων με χρήση σωματιδιακών μεθόδων. Επίσης, παρουσιάζεται η δυνητική καθιέρωσή των σωματιδιακών μεθόδων ως ντετερμινιστική μεθοδολογία επίλυσης.

Contents

1. Introduction and literature review	1
1.1 Origin of kinetic theory	1
1.2 Knudsen number and flow regimes	1
1.3 Particle in cell methods	5
1.4 Thesis objectives and structure	6
2. Basic concepts of kinetic theory	8
2.1 Boltzmann equation	8
2.2 Kinetic models	9
2.3 Boundary conditions	10
2.4 Macroscopic quantities	11
2.5 Projection procedure	12
2.5.1 Projection on \mathbf{x} and \mathbf{z} components	14
2.5.2 Projection on \mathbf{z} component	18
3. Description and formulation of the method	20
3.1 Formulation of the non-linear BE	20
3.2 Basic description of the PIC method	21
3.3 Time dependent flows	22
3.4 Flows with external force fields	24
3.5 Steady state flows	25
3.6 PIC codes	25
3.5.1 The P1V1 code	26
3.5.2 The P1V2 code	27
3.5.3 Extensions of P1V1 and P1V2 codes	29
3.6 Advantages of PIC codes	30
4. Flow configuration and basic parameters of prototype problems	31
4.1 Non-linear Couette flow	31
4.2 Non-linear Fourier flow	32
4.3 Non-linear Poiseuille flow	33
4.4 Free molecular solutions	34
5. Results and discussion	37
5.1 Non-linear Couette flow	37
5.2 Non-linear Fourier flow	38
5.3 Poiseuille flow	39
6. Concluding remarks	48
References	49

1. Introduction and literature review

1.1 Origin of kinetic theory

Kinetic theory first originated in 1738 when Daniel Bernoulli stated in his book *Hydrodynamica* [1] that gases consist of large amounts of molecules travelling in all directions, that pressure is the force exerted by those molecules to a surface during a collision and that heat is just the kinetic energy of the molecules. Great advances in kinetic theory came much later, when in 1878 Clausius [2] introduced the mean free path and Maxwell in 1860 [3] who laid the road for a statistical description of gasses, introducing the concept of the velocity distribution function, a tool that could be used to compute the probability of finding a molecule in a certain range of velocities. Although Maxwell came very close to extraction the expression for the evolution of this function (the Boltzmann equation), it was Boltzmann in 1872 [4] that made the final steps to its derivation and the expressions is accorded to him.

Kinetic theory approaches the gas not as a continuous medium, by rather than a huge amount of atoms, moving randomly in all directions and colliding with each other. This is the reason that in the beginning of the 20th century it was criticized, as atoms were considered by many physicists to be purely hypothetical. It was after the first papers on Brownian motion [5,6], where accurate predictions based on kinetic theory were made, that the scientific community accepted it. Initially, kinetic theory was utilized in order to obtain closed form expressions for the transport coefficients, rather than simulate problems. In the second part of the 20th century, following the development of computers some simple problems were simulated. As will be discussed in the next section, kinetic theory is applied in certain cases where the conventional approaches fail, mainly in vacuum conditions or for phenomena taking place in very small dimensions. Recently, kinetic theory was even utilized to study historical processes [7].

1.2 Knudsen number and flow regimes

One of the main advantages of kinetic theory is that the only assumption that needs to be made is the specification of the intermolecular interaction model, instead of the transport coefficients needed for conventional CFD approaches. However, kinetic simulations are associated with high computational load, and are used when absolutely necessary and that is when the gas is very far from equilibrium. The dimensionless parameter that quantifies the departure from local equilibrium is the Knudsen number.

The Knudsen number is defined as the ratio of the mean free path of the molecules over a characteristic length of the problem [8]

$$Kn = \frac{\lambda}{L} \quad (1.1)$$

The mean free path for the Hard Sphere model for a single gas can be expressed as [8]

$$\lambda = \frac{m}{\sqrt{2}\pi d^2 \rho} \quad (1.2)$$

where m is the molecular mass, d is the diameter of the molecule and ρ is the gas mass density. It is seen that for a specific gas the mean free path is a function only of density, and is inversely proportional to it. The Knudsen number is a measure of the gas rarefaction and a measure of the departure from local equilibrium.

Table 1.1: Direct and cross effects.

	Heat flux	Momentum flux	Mass flux
∇T	Heat conduction	Thermal creep	Thermal diffusion
∇P	Mechanocaloric effect	Poiseuille flow	Baroeffect
∇C	Duffour effect	Diffusion baroeffect	Diffusion flow

The Knudsen number is related to other important dimensionless parameters, such as the rarefaction parameter

$$\delta = \frac{PL}{\mu v_0} = \frac{\sqrt{\pi}}{2Kn} \quad (1.3)$$

and the Mach and Reynolds numbers [8]

$$Kn = \frac{Ma}{Re} \sqrt{\frac{\gamma\pi}{2}} \quad (1.4)$$

where P is the gas pressure, μ is the dynamic viscosity, $v_0 = \sqrt{2k_B T / m}$ is the most probable velocity, k_B is the Boltzmann constant and γ is the ratio of the specific heats of the gas.

According to the Knudsen number the flow regimes can be defined, as shown in Table 1.2. The Boltzmann equation, although valid in the whole range of the Knudsen number, is utilized only in the transition and free molecular regimes because of the high computational cost it requires.

When the Knudsen number is small and the flow is in the continuum regime, the macroscopic approach of the Euler and Navier Stokes equations can be used with very good accuracy. As the Knudsen number is increased and we move to the Slip regime, the no-slip boundary conditions associated with the Navier Stokes equations start to collapse. This can be treated with velocity slip and temperature jump boundary conditions [9], and the range of their application is extended. In those regimes the flow is near local equilibrium.

As the Knudsen number is further increased and the flow further departs from local equilibrium, the Newton, Fourier and Fick laws do not hold and the continuum approach collapses. It is in those regimes, the transition and free molecular, that very interesting non-equilibrium phenomena start to appear, and the flow can only be simulated using kinetic approaches [10,11].

Table 1.2: The flow regimes according to the Knudsen number.

Range of Kn	Regime	Governing Equations	Numerical approach
$Kn \rightarrow 0$	Continuum (inviscid)	Euler	Typical CFD schemes
$Kn < 10^{-3}$	Continuum (viscous)	Navier Stokes	
$10^{-3} < Kn < 10^{-1}$	Slip (viscous)	Navier Stokes with slip boundary conditions, Generalized equations.	
$10^{-1} < Kn < 10$	Transition (Knudsen)	Boltzmann Kinetic models	Analytical methods, Variational methods, Discrete velocity method Integro-moment method DSMC
$10 < Kn$	Free molecular	Boltzmann and kinetic models without collisions	Method of characteristics Test particle Monte Carlo

If we consider the three driving forces acted on gases being temperature gradient, pressure gradient and concentration gradient, then the results of those forces according to continuum approaches will be heat flux, momentum flux and mass flux respectively. Those are called direct effects. In flows far from local equilibrium six more effects are present, the cross effects. They are shown in Table 1.1. The mechanocaloric and Duffour effects give a heat flux due to pressure and concentration gradients respectively, thermal creep and diffusion baroeffect give momentum flux due to temperature and concentration gradients and finally the thermal diffusion and baroeffect give mass fluxes due to temperature and pressure gradients. Those effects are beyond the range of the continuum models, can however be modeled by kinetic approaches and although negligible at small Knudsen numbers, are very important in rarefied flows.

The direct solution of the Boltzmann equation is a very hard and computationally demanding process. To overcome this, certain methods are used in order to obtain kinetic solutions without solving the exact Boltzmann equation. One of them is the use of kinetic models, the most well-known are the BGK [12], the Shakhov [13] and Ellipsoidal [14] models for monatomic single gas flows, the Rykov [15] and Holway [16] models for polyatomic single gas flows and the McCormack [17] model for gas mixtures. In order for a model to be accepted it must satisfy the collision invariants, satisfy the H-theorem and provide the correct expressions for the transport coefficients.

Another very widely used method for the simulation of such flows is the Direct Simulation Monte Carlo method (DSMC) [10]. This is a stochastic method, in contrast to the direct solution of the BE or model equations. For the simulation the flow domain is discretized and a big number of fictional (simulator) particles are distributed on the field, each corresponding to a large number of real particles. Then the real motion of particles is divided into two parts, the free motion according to a distance proportional to their velocities and the time step, and a collision part where the collisions are simulated in a stochastic manner. This way the free motion and the collisions are decoupled, during the time step. The macroscopic quantities are sampled for a large number of time steps, and are calculated using the simulator particles' microscopic quantities. It should be noted that since it is a stochastic method, it suffers from statistical noise and a lot of work is done in order to decrease it [18].

A number of methods have been proposed, using high-order equations [19] derived from the BE. Those methods are able to simulate flows in the slip and early transition regimes, capturing effects that are beyond the NSF (Navier-Stokes-Fourier) analysis. The most known

of them are the Burnett equations. Those methods have some known problems, like stability issues, and can be misleading when used in the whole transition regime.

1.3 Particle in cell methods

Particle-in-cell is a class of numerical methods used to solve partial differential equations. In those methods the equation to be solved is decomposed into auxiliary problems, typically one in a Lagrangian frame and one in Eulerian. The phase space is discretized and unlike other methods, the solution is not performed on the nodes or elements of the computational mesh. Instead, a large number of fictional (simulator) particles is created and their motion is tracked on a Lagrangian frame. Each of those particles carries the information of the quantities of interest. The particles can interact with the Eulerian grid through average fields (PM, particle-mesh interaction), with other particles (PP, particle-particle) as in cases of charged plasma, or include both types of interaction (PP-PM or P³M). In all cases considered in this work the PM interaction is used. The solution is then performed following some steps, the motion of all particles, the interaction of particles with the mesh or other particles, the calculation of field variables (e.g. Maxwell equations for plasma) and finally the weighting of the particle microscopic properties in order to derive the macroscopic quantities of interest [20].

Particle-in-cell methods are well known in the scientific community. They offer a degree of intuition and are usually straightforward to implement, a fact that made those methods quickly popular as they provided solutions to complex effects based on their imitative properties. They were very successful in plasma simulation, and magnetohydrodynamics for applications involving tokamaks [21], and are the leading method for simulating such problems. Initially those methods were oriented to solving problems with great bulk deformation, strong shears, instabilities on the interfaces of various media, turbulent mixing and other cases where finite difference schemes proved to be inapplicable [22]. Great progress was made when the splitting up into the auxiliary problems scheme was introduced [23], and great steps for the computational aerodynamics were made when the “large” particle method was introduced [24] that enabled simulation of transonic flows past bodies and two-phase flows.

In the field of rarefied gas dynamics, particle in cell methods were developed in the sixties-seventies, at the time when rarefied gas dynamics became a separate branch of engineering, due to the development of space science and vacuum technologies. Statistical particle in cell methods were developed, as imitation algorithms for such flows, mostly by

G.A. Bird [10] and contribution was also made by O.M. Belotserkovsky and B. Ye. Yanitsky [25,26]. Since then, this statistical particle-in-cell method (DSMC) is still used massively for engineering applications involving rarefied gases.

1.4 Thesis objectives and structure

Rarefied gas flow simulation is an emerging field of engineering. There is an increasing interest in the fields of microfluidics [27] and vacuum packed MEMS [28,29] as well as micropumps [30,31], microactuators/microsensors [32,33], and vacuum systems simulation. Only recently however, have large scale simulations become possible, due to the high computational cost associated with it, and as time goes by more and more complex simulations are demanded. Nowadays, the most widely used method used to tackle complex engineering problems involving rarefied flows is the DSMC method, which however suffers from statistical noise, and in some cases (e.g. creeping flows) fails to correctly reproduce the flow field due to this noise.

Particle-in-cell methods provide great advantages as the simulation of complex geometries becomes easier and since they are imitative techniques, the particle interaction becomes easier to model (e.g. external fields). The large linear systems that are inherent in finite elements methods do not exist in PIC methods, decreasing the computational cost. Particle-in-cell methods are not new in rarefied gas dynamics, as the DSMC itself is such a method. However, DSMC suffers from certain problems that are not present in deterministic methods. On the other hand, deterministic techniques of solving rarefied flows, using the typical numerical schemes, are hard or very computational demanding to implement on complicated problems. An effort is made in the present work to develop a methodology for the deterministic simulation of rarefied gas flows, using particle-in-cell methods. This could potentially increase the range of application of deterministic techniques, to problems currently tackled by DSMC. In the context of the present work, some basic algorithms are developed and the general guidelines of such a solver are given, while a few simple problems are simulated in order to verify and benchmark the method.

The thesis is outlined as follows:

- The basic concepts of kinetic theory are given in Chapter 2. The Boltzmann equation, along with the kinetic models, boundary conditions and macroscopic quantities are presented and the mathematical manipulation of the equations to be solved is made.

- The description of the PIC method used in the present work is presented in Chapter 3. The basic aspects of the method as well as the formulation of the test algorithms are given.
- In Chapter 4 the formulation of the benchmark problems is presented.
- In Chapter 5 the results of the benchmark problems are presented and the comparison with published results is made.
- Closing the thesis some concluding remarks are made in Chapter 6.

2. Basic concepts of kinetic theory

2.1 Boltzmann equation

Kinetic theory simulations are based on the velocity distribution function $f(\mathbf{r}, \boldsymbol{\xi}, t)$, where \mathbf{r} is the physical space position vector, $\boldsymbol{\xi}$ is the molecular velocity vector and t is time. The velocity distribution function (or simply distribution function) is defined so that $f(\mathbf{r}, \boldsymbol{\xi}, t) d\mathbf{r} d\boldsymbol{\xi}$ is the expected number of particles that are in the physical space element of volume $d\mathbf{r}$ around \mathbf{r} and have velocities in $d\boldsymbol{\xi}$ around $\boldsymbol{\xi}$ at time t . The six dimensional space formed by the three physical space vectors and the three molecular velocity vectors is called the phase space and the quantity $d\mathbf{r} d\boldsymbol{\xi}$ is a phase space differential element. The distribution function is a fundamental quantity in kinetic theory and all macroscopic quantities of interest can be derived from the distribution function. As it can be seen the distribution function, in the general case, depends on seven independent variables and this makes simulations hard and computationally demanding. The evolution equation for the distribution function is the Boltzmann equation (BE), that for the case of monatomic single gases can be written as [8]

$$\underbrace{\frac{\partial f}{\partial t}}_{\text{rate of change}} + \underbrace{\boldsymbol{\xi} \frac{\partial f}{\partial \mathbf{r}}}_{\text{rate of change due to free motion}} + \underbrace{\mathbf{F} \frac{\partial f}{\partial \boldsymbol{\xi}}}_{\text{rate of change due to field forces}} = \underbrace{\int_{-\infty}^{+\infty} \int_0^{4\pi} (f_1^* f^* - f_1 f) \mathbf{c}_r \sigma d\Omega d\boldsymbol{\xi}_1}_{\text{rate of change due to collisions}} = J(f) \quad (2.1)$$

The left hand side of the BE is the streaming term, the change due to the free motion and the right hand side is the collision term, the change due to collisions. The collision integral gives the rate of change due to collisions of the particles inside the phase space element $d\mathbf{r} d\boldsymbol{\xi}$ with particles of all other phase space elements $d\mathbf{r} d\boldsymbol{\xi}_1$. The quantities with the superscript (*) are the post collision quantities and those with the subscript (1) refer to the phase space elements $d\mathbf{r} d\boldsymbol{\xi}_1$. The relative velocity of the colliding particles is denoted as $\mathbf{c}_r = \boldsymbol{\xi} - \boldsymbol{\xi}_1$, while σ denotes the differential cross section and $d\Omega$ is the differential element of the solid angle in which the molecule will scatter after the collision. Those two parameters (σ and $d\Omega$) are the only parameters that need to be specified in advance and they are derived from the molecular interaction model chosen, the most common being the Hard Sphere, Inverse Power Law, Variable Hard Sphere, Variable Soft Sphere, Generalized Hard Sphere and Generalized Soft Sphere models. This is one of the advantages of kinetic theory, the in order

to simulate the flow we do not need to specify any transport coefficients, but instead only the molecular interaction model.

Deriving the BE two main assumptions have to be made, both regarding the collision part. The first assumption is that only binary collisions, that is collisions between two particles, are taken into account. This limits the applicability of the BE to dilute gasses (a gas is considered dilute when the distance between molecules is much larger than the molecular diameter). It is noted that gases in atmospheric pressure are dilute. The second assumption is the molecular chaos or Stosszahlansatz, which states that the velocities of the colliding molecules are uncorrelated.

One particular solution of the BE when external forces are absent and for an equilibrium state is the global Maxwellian distribution

$$f^M = \frac{N}{\left(2\pi \frac{k_B}{m} T\right)^{3/2}} \exp \left[-\frac{(\xi - U)^2}{2 \frac{k_B}{m} T} \right] \quad (2.2)$$

where N , T , U are the constant number density, temperature and velocity while k_B , m are the Boltzmann constant and molecular mass respectively. When the macroscopic quantities N , T , U are not constant but depend on time and physical space then the distribution of the same form is the local Maxwellian distribution.

2.2 Kinetic models

As can be seen in Eq. (2.1) the collision part of the BE is, in the general case, given by a five-fold integral. The simulation of gas flows using the BE in the form given in Eq. (2.1) is a very cumbersome and computationally demanding task, because of this complex collision part. In order to simplify the simulation it is common to replace the collision integral with simpler expressions, the kinetic models. In essence kinetic models provide a relaxation to the collision term and have proven to be adequately accurate for flow simulation.

The most basic and well known kinetic model is the BGK model, which is given by [12]

$$J(f) = \frac{P}{\mu} (f^M - f) \quad (2.3)$$

where P is the local pressure, μ is the viscosity at local temperature and f^M is the local Maxwellian distribution. This model, although relatively simple, has been extensively used to model isothermal gas flows, with considerable success. The main drawback of the BGK model is that it cannot provide the correct expressions for viscosity and thermal conductivity

coefficients simultaneously, as it yields a Prandtl number of $Pr=1$ instead of $2/3$ for ideal gases, making it unsuitable for non-isothermal flows.

An extension of the BGK model, able to handle non-isothermal flows is the Shakhov model, which provides the correct value of the Prandtl number and has been used extensively for non-isothermal flows. The Shakhov model is given by [13]

$$J(f) = \frac{P}{\mu} (f_{eq}^S - f) \quad (2.4)$$

where

$$f_{eq}^S = f^M \left[1 + \frac{2}{5} \frac{m(1-Pr)}{N(k_B T)^2} \mathbf{Q} \cdot (\boldsymbol{\xi} - \mathbf{U}) \left(\frac{m(\boldsymbol{\xi} - \mathbf{U})^2}{2k_B T} - \frac{5}{2} \right) \right] \quad (2.5)$$

where Pr is the Prandtl number and \mathbf{Q} is the heat flux vector. Both of the above models, BGK and Shakhov are limited to monatomic gas flows.

2.3 Boundary conditions

The boundary conditions for flows simulated using the BE are part of the solution. Their main objective is to correlate the distribution of the molecules departing from the boundary with that of the incoming molecules. The most widely used type of boundary conditions is the Maxwell diffuse-specular. In the case of purely diffuse boundary conditions the distribution of the molecules departing from the boundary is in the form of the Maxwellian distribution characterized by the wall temperature and velocity. Specular reflection assumes that molecules arriving to the boundary collide with it in an elastic way, and are reflected without exchanging energy with the boundary. If we consider \mathbf{n} as unit normal to the boundary vector with direction towards the flow field, we can denote the incoming distribution as $f^-(\boldsymbol{\xi}')$ when $\boldsymbol{\xi}' \cdot \mathbf{n} < 0$ and the outgoing as $f^+(\boldsymbol{\xi})$ when $\boldsymbol{\xi} \cdot \mathbf{n} > 0$. A general expression for the boundary conditions is [8]

$$f^+(\boldsymbol{\xi}) = - \int_{\boldsymbol{\xi}' \cdot \mathbf{n} < 0} \frac{\boldsymbol{\xi}' \cdot \mathbf{n}}{\boldsymbol{\xi} \cdot \mathbf{n}} W(\boldsymbol{\xi}' \rightarrow \boldsymbol{\xi}) f^-(\boldsymbol{\xi}') d\boldsymbol{\xi}' \quad (2.6)$$

where $W(\boldsymbol{\xi}' \rightarrow \boldsymbol{\xi})$ is the scattering kernel and it is the probability that a molecule arriving at the boundary with velocity $\boldsymbol{\xi}'$ will depart with velocity $\boldsymbol{\xi}$.

In the case of specular reflection only the velocity component normal to the boundary will change (and become opposite) that is

$$f^+(\boldsymbol{\xi}) = f^-(\boldsymbol{\xi} - 2(\boldsymbol{\xi} \cdot \mathbf{n})\mathbf{n}) \quad (2.7)$$

leading to the scattering kernel

$$W_s(\xi' \rightarrow \xi) = \delta[\xi' - \xi + 2(\xi \cdot \mathbf{n})\mathbf{n}] \quad (2.8)$$

where δ is the Dirac function according to $\int \delta(\mathbf{r} - \mathbf{a})\varphi(\mathbf{r})d\mathbf{r} = \varphi(\mathbf{a})$.

In the case of purely diffuse boundary conditions, the outgoing distribution is of the form of the Maxwell distribution characterized by the wall conditions,

$$f^+(\xi) = \frac{N_w}{\left(2\pi \frac{k_B}{m} T_w\right)^{3/2}} \exp\left[-\frac{(\xi - U_w)^2}{2 \frac{k_B}{m} T_w}\right] \quad (2.9)$$

where T_w is the boundary temperature, U_w is the boundary velocity and N_w is a parameter ensuring the impermeability condition. The above expression gives the scattering kernel

$$W_d(\xi' \rightarrow \xi) = \frac{1}{2\pi} \xi \cdot \mathbf{n} \frac{m}{(k_B T_w)^{3/2}} \exp\left[-\frac{(\xi - U_w)^2}{2 \frac{k_B}{m} T_w}\right] \quad (2.10)$$

In practice the boundary interaction is not purely specular neither purely diffusive. It is more accurate to assume that a portion a of the molecules is reflected diffusively and the remaining $(1-a)$ undergoes specular reflection, leading to the diffuse-specular scattering kernel

$$W(\xi' \rightarrow \xi) = aW_d(\xi' \rightarrow \xi) + (1-a)W(\xi' \rightarrow \xi). \quad (2.11)$$

2.4 Macroscopic quantities

Macroscopic quantities of practical interest can be obtained as moments of the distribution function using the following expressions [8]

$$\text{Number density } N(\mathbf{r}, t) = \int_{R^3} f(\mathbf{r}, \xi, t) d\xi \quad (2.12)$$

$$\text{Velocity vector } \mathbf{U}(\mathbf{r}, t) = \frac{1}{N(\mathbf{r}, t)} \int_{R^3} \xi f(\mathbf{r}, \xi, t) d\xi \quad (2.13)$$

$$\text{Stress tensor } P_{ij}(\mathbf{r}, t) = m \int_{R^3} (\xi_i - U_i)(\xi_j - U_j) f(\mathbf{r}, \xi, t) d\xi \quad (2.14)$$

$$\text{Temperature } T(\mathbf{r}, t) = \frac{m}{3k_B N(\mathbf{r}, t)} \int_{R^3} (\xi - U)^2 f(\mathbf{r}, \xi, t) d\xi \quad (2.15)$$

$$\text{Heat flux vector } \mathbf{Q}(\mathbf{r}, t) = \frac{m}{2} \int_{R^3} (\xi - U)^2 (\xi - U) f(\mathbf{r}, \xi, t) d\xi \quad (2.16)$$

2.5 Projection procedure

Although the distribution function can be a function of only one or two physical space dimensions, it still is a function of all three molecular velocity components. In order to reduce the computational cost it is possible, depending on the problem to be simulated, to eliminate one or two molecular velocity components using the projection procedure. During the projection procedure the kinetic model equation along with the expressions for the macroscopic quantities and the boundary conditions are accordingly integrated in order to eliminate the dependence on some of the molecular velocity components. Then instead of the kinetic equation a system of integrodifferential equations has to be solved, increasing the complexity, but the computational cost is reduced by at least one order of magnitude. Of course during the projection procedure some information is lost, but this is of no practical interest. Before applying the projection procedure it is convenient to introduce the following dimensionless quantities

$$\mathbf{r} = \frac{\mathbf{r}'}{L}, \tau = \frac{T}{T_0}, n = \frac{N}{N_0}, \mathbf{u} = \frac{\mathbf{U}}{v_0}, \boldsymbol{\zeta} = \frac{\boldsymbol{\xi}}{v_0}, v_0 = \sqrt{2 \frac{k_B}{m} T_0}, \mathbf{q} = \frac{\mathbf{Q}}{N_0 k_B T_0 u_0}, p_{ij} = \frac{P_{ij}}{N_0 k_B T_0} \quad (2.17)$$

$$g = f \frac{u_0^3}{N_0}$$

where T_0, N_0 are the reference temperature and number density respectively, while the reference pressure P_0 is taken from the state equation as $P_0 = N_0 k_B T_0$. The reference speed is the mean thermal velocity v_0 at reference temperature and g denotes the dimensionless distribution function.

Two cases of the projection procedure will be shown here. In the first case, two components (z, x) of the molecular velocity will be eliminated and in the second only one component (z) . In both cases the distribution function will only depend on one direction (y) of the physical space and the steady state equation will be used. Under those assumptions the BE can be written as

$$\xi_y \frac{\partial f}{\partial y} + F_x \frac{\partial f}{\partial \xi_x} = J(f) \quad (2.18)$$

if we introduce the dimensionless quantities of Eq. (2.17) then the BE is written as

$$\zeta_y \frac{\partial g}{\partial y} + \bar{F} \frac{\partial g}{\partial \zeta_x} = \bar{J}(g) \quad (2.19)$$

where $\bar{F} = F_x \frac{L}{v_0^2}$ is the inverse of the Froude number and $\bar{J}(g)$ is the dimensionless collision operator. The dimensionless collision operator for the BGK and Shakhov models can be written as

$$\bar{J}_{BGK}(g) = \delta(g^M - g) \quad (2.20)$$

and

$$\bar{J}_s(g) = \delta(g^S - g) \quad (2.21)$$

where g^M is the dimensionless Maxwellian distribution and g^S is the dimensionless Shakhov equilibrium distribution given by

$$g^M = \frac{n}{(\pi\tau)^{3/2}} \exp\left[-(\boldsymbol{\zeta} - \mathbf{u})^2 / \tau\right] \quad (2.22)$$

and

$$g^S = g^M \left(1 + \frac{4}{5} \frac{(1 - \text{Pr})}{n\tau^2} \mathbf{q} \cdot (\boldsymbol{\zeta} - \mathbf{u}) \left(\frac{(\boldsymbol{\zeta} - \mathbf{u})^2}{\tau} - \frac{5}{2} \right) \right) \quad (2.23)$$

The parameter δ in Eqs. (2.20) and (2.21) is the local rarefaction parameter, which is proportional to the inverse of the Knudsen number, and is given by

$$\delta = \frac{PL}{\mu v_0} \quad (2.24)$$

and is connected to the reference rarefaction parameter $\delta_0 = \frac{P_0 L}{\mu_0 v_0}$ by

$$\delta = \delta_0 n \tau^{1-\omega} \quad (2.25)$$

where ω is the viscosity index, $\mu = \mu_0 \left(\frac{T}{T_0} \right)^\omega$, and the two limiting cases of $\omega = 0.5$ and 1

correspond to hard sphere and Maxwell molecules respectively.

The dimensionless expressions for the macroscopic quantities are summarized bellow

$$\text{Number density } n(\mathbf{r}) = \int_{R^3} g(\mathbf{r}, \boldsymbol{\zeta}) d\boldsymbol{\zeta} \quad (2.26)$$

$$\text{Velocity vector } \mathbf{u}(\mathbf{r}) = \frac{1}{n(\mathbf{r})} \int_{R^3} \boldsymbol{\zeta} g(\mathbf{r}, \boldsymbol{\zeta}) d\boldsymbol{\zeta} \quad (2.27)$$

$$\text{Stress tensor } p_{ij}(\mathbf{r}) = 2 \int_{R^3} (\zeta_i - u_i)(\zeta_j - u_j) g(\mathbf{r}, \boldsymbol{\zeta}) d\boldsymbol{\zeta} \quad (2.28)$$

$$\text{Temperature } \tau(\mathbf{r}) = \frac{2}{3n(\mathbf{r})} \int_{R^3} (\boldsymbol{\zeta} - \mathbf{u})^2 g(\mathbf{r}, \boldsymbol{\zeta}) d\boldsymbol{\zeta} \quad (2.29)$$

$$\text{Heat flux vector } \mathbf{q}(\mathbf{r}) = \int_{R^3} (\boldsymbol{\zeta} - \mathbf{u})^2 (\boldsymbol{\zeta} - \mathbf{u}) g(\mathbf{r}, \boldsymbol{\zeta}) d\boldsymbol{\zeta} \quad (2.30)$$

Finally the expressions for the boundary conditions become

$$g^+ = \frac{n_w}{(\pi\tau_w)^{3/2}} \exp\left[-\frac{(\boldsymbol{\zeta} - \mathbf{u}_w)^2}{\tau_w}\right] \text{ for } \boldsymbol{\zeta} \cdot \mathbf{n} > 0 \quad (2.31)$$

with

$$n_w = -\frac{\int_{\boldsymbol{\zeta} \cdot \mathbf{n} < 0} (\boldsymbol{\zeta} \cdot \mathbf{n}) g^-(\mathbf{r}, \boldsymbol{\zeta}) d\boldsymbol{\zeta}}{\int_{\boldsymbol{\zeta} \cdot \mathbf{n} > 0} \frac{(\boldsymbol{\zeta} \cdot \mathbf{n})}{(\pi\tau_w)^{3/2}} \exp\left[-\frac{(\boldsymbol{\zeta} - \mathbf{u}_w)^2}{\tau_w}\right] d\boldsymbol{\zeta}} \quad (2.32)$$

The projection procedure will now be applied on the dimensionless BE as well as the expressions for the macroscopic quantities and boundary conditions. Two different projection procedures will be shown here, in the first one two components (z, x) of the molecular velocity will be eliminated, while in the second only one (z) .

2.5.1 Projection on x and z components

In order to eliminate those two components of the molecular velocity we need to specify the following reduced distribution functions

$$Y(y, \zeta_y) = \int_{-\infty}^{+\infty} \int_{-\infty}^{+\infty} g(y, \zeta_x, \zeta_y, \zeta_z) d\zeta_x d\zeta_z \quad (2.33)$$

$$\Phi(y, \zeta_y) = \int_{-\infty}^{+\infty} \int_{-\infty}^{+\infty} \zeta_x g(y, \zeta_x, \zeta_y, \zeta_z) d\zeta_x d\zeta_z \quad (2.34)$$

$$X(y, \zeta_y) = \int_{-\infty}^{+\infty} \int_{-\infty}^{+\infty} [\zeta_x^2 + \zeta_z^2] g(y, \zeta_x, \zeta_y, \zeta_z) d\zeta_x d\zeta_z \quad (2.35)$$

$$\Psi(y, \zeta_y) = \int_{-\infty}^{+\infty} \int_{-\infty}^{+\infty} \zeta_x^2 g(y, \zeta_x, \zeta_y, \zeta_z) d\zeta_x d\zeta_z \quad (2.36)$$

and

$$\Omega(y, \zeta_y) = \int_{-\infty}^{+\infty} \int_{-\infty}^{+\infty} \zeta_x [\zeta_x^2 + \zeta_z^2] g(y, \zeta_x, \zeta_y, \zeta_z) d\zeta_x d\zeta_z. \quad (2.37)$$

Then we apply the following integral operators

$$\iint (\cdot) d\zeta_x d\zeta_z \quad (2.38)$$

$$\iint (\cdot) \zeta_x d\zeta_x d\zeta_z \quad (2.39)$$

$$\iint (\cdot) (\zeta_x^2 + \zeta_z^2) d\zeta_x d\zeta_z \quad (2.40)$$

$$\iint (\cdot) \zeta_x^2 d\zeta_x d\zeta_z \quad (2.41)$$

$$\iint (\cdot) \zeta_x (\zeta_x^2 + \zeta_z^2) d\zeta_x d\zeta_z \quad (2.42)$$

on the kinetic equation (2.19) which, for this case, is taken omitting the external acceleration term. For the BGK model this equation becomes

$$\zeta_y \frac{\partial g}{\partial y} = \delta (g^M - g) = \delta_0 n \tau^{1-\omega} (g^M - g) \quad (2.43)$$

and if we apply the integral operators (2.38)-(2.42) we get the following system for the reduced distribution functions

$$\zeta_y \frac{\partial Y}{\partial y} = \delta_0 n \tau^{1-\omega} (Y^M - Y) \quad (2.44)$$

$$\zeta_y \frac{\partial \Phi}{\partial y} = \delta_0 n \tau^{1-\omega} (\Phi^M - \Phi) \quad (2.45)$$

$$\zeta_y \frac{\partial X}{\partial y} = \delta_0 n \tau^{1-\omega} (X^M - X) \quad (2.46)$$

$$\zeta_y \frac{\partial \Psi}{\partial y} = \delta_0 n \tau^{1-\omega} (\Psi^M - \Psi) \quad (2.47)$$

$$\zeta_y \frac{\partial \Omega}{\partial y} = \delta_0 n \tau^{1-\omega} (\Omega^M - \Omega) \quad (2.48)$$

where the reduced Maxwellians are given by

$$Y^M = \frac{n}{\sqrt{\pi\tau}} \exp\left(-\frac{(\zeta_y - u_y)^2}{\tau}\right) \quad (2.49)$$

$$\Phi^M = \frac{n}{\sqrt{\pi\tau}} u_x \exp\left(-\frac{(\zeta_y - u_y)^2}{\tau}\right) = Y^M u_x \quad (2.50)$$

$$X^M = \frac{n}{\sqrt{\pi\tau}} [u_x^2 + \tau] \exp\left(-\frac{(\zeta_y - u_y)^2}{\tau}\right) = Y^M [u_x^2 + \tau] \quad (2.51)$$

$$\Psi^M = \frac{n}{2\sqrt{\pi\tau}} [2u_x^2 + \tau] \exp\left(-\frac{(\zeta_y - u_y)^2}{\tau}\right) = Y^M \frac{[2u_x^2 + \tau]}{2} \quad (2.52)$$

$$\Omega^M = \frac{n}{\sqrt{\pi\tau}} u_x [u_x^2 + 2\tau] \exp\left(-\frac{(\zeta_y - u_y)^2}{\tau}\right) = \Phi^M [u_x^2 + 2\tau] \quad (2.53)$$

For the Shakhov model, the kinetic equation becomes

$$\zeta_y \frac{\partial g}{\partial y} = \delta_0 n \tau^{1-\omega} (g^S - g) \quad (2.54)$$

and applying the integral operators (2.38)-(2.42) to this equation and setting $\text{Pr} = 2/3$ we get the following system for the reduced distribution functions

$$\zeta_y \frac{\partial Y}{\partial y} = \delta_0 n \tau^{1-\omega} \left(Y^M \left[1 + \frac{2\zeta_y q_y (2\zeta_y^2 - 3\tau)}{15n\tau^3} \right] - Y \right) \quad (2.55)$$

$$\zeta_y \frac{\partial \Phi}{\partial y} = \delta_0 n \tau^{1-\omega} \left(\Phi^M \left[1 + \frac{4\zeta_y^3 q_y u_x + 2\zeta_y (\zeta_y q_x - 3q_y u_x) \tau - q_x \tau^2}{15n u_x \tau^3} \right] - \Phi \right) \quad (2.56)$$

$$\zeta_y \frac{\partial X}{\partial y} = \delta_0 n \tau^{1-\omega} \left(X^M \left[1 + \frac{4\zeta_y^2 q_x u_x \tau - 2q_x u_x \tau^2 + 4\zeta_y^3 q_y (u_x^2 + \tau) - 2\zeta_y q_y \tau (3u_x^2 + \tau)}{15n (u_x^2 + \tau) \tau^3} \right] - X \right) \quad (2.57)$$

$$\zeta_y \frac{\partial \Psi}{\partial y} = \delta_0 n \tau^{1-\omega} \left(\Psi^M \left[1 + \frac{8\zeta_y^2 q_x u_x \tau - 4q_x u_x \tau^2 + 4\zeta_y^3 q_y (2u_x^2 + \tau) - 2\zeta_y q_y \tau (6u_x^2 + \tau)}{15n (2u_x^2 + \tau) \tau^3} \right] - \Psi \right) \quad (2.58)$$

$$\zeta_y \frac{\partial \Omega}{\partial y} = \delta_0 n \tau^{1-\omega} (\Omega^M [1 + \mathcal{K}] - \Omega) \quad (2.59)$$

where

$$\mathcal{K} = \frac{q_x \tau^2 (-3u_x^2 + 2\tau) + 4\zeta_y^3 q_y u_x (u_x^2 + 2\tau) + (2\zeta_y^2 q_x \tau - 2\zeta_y q_y u_x \tau) (3u_x^2 + 2\tau)}{15n u_x (u_x^2 + 2\tau) \tau^3}$$

The expressions for the macroscopic quantities (2.26)-(2.30), in terms of the reduced distribution functions can be written as

$$n(y) = \int_{-\infty}^{+\infty} Y(y, \zeta_y) d\zeta_y \quad (2.60a)$$

$$u_x(y) = \frac{1}{n} \int_{-\infty}^{+\infty} \Phi(y, \zeta_y) d\zeta_y \quad (2.60b)$$

$$u_y(y) = \frac{1}{n} \int_{-\infty}^{+\infty} \zeta_y Y(y, \zeta_y) d\zeta_y \quad (2.60c)$$

$$\tau(y) = \frac{2}{3n} \int_{-\infty}^{+\infty} [Y\zeta_y^2 + X] d\zeta_y - \frac{2}{3} u_x^2(y) - \frac{2}{3} u_y^2(y) \quad (2.60d)$$

$$q_x(y) = \int_{-\infty}^{+\infty} (\Omega - 2u_x\Psi + 3u_x^2\Phi - u_x^3Y + \zeta_y^2\Phi - u_x\zeta_y^2Y - u_xX - 2u_y\zeta_y\Phi + 2u_xu_y\zeta_yY - u_y^2u_xY) d\zeta_y \quad (2.60e)$$

$$q_y(y) = \int_{-\infty}^{+\infty} (\zeta_y^3Y + \zeta_yX - 2u_x\zeta_y\Phi - u_yX - 3u_y\zeta_y^2Y + 2u_xu_y\Phi + 3u_y^2\zeta_yY - u_x^2u_yY + u_x^2\zeta_yY - u_y^3Y) d\zeta_y \quad (2.60f)$$

$$p_{xy}(y) = 2 \int_{-\infty}^{+\infty} (\zeta_y\Phi - u_y\Phi - u_x\zeta_yY + u_xu_yY) d\zeta_y \quad (2.60g)$$

$$p_{xx}(y) = 2 \int_{-\infty}^{+\infty} \Psi d\zeta_y - u_x^2\rho \quad (2.60h)$$

$$p_{yy}(y) = 2 \int_{-\infty}^{+\infty} (\zeta_y - u_y)^2 Y d\zeta_y \quad (2.60i)$$

$$p_{zz}(y) = 2 \int_{-\infty}^{+\infty} [X - \Psi] d\zeta_y \quad (2.60j)$$

The outgoing distribution at the boundaries after the projection procedure, for each of the reduced distribution functions, is of the form of the corresponding reduced Maxwellian distribution Eqs.(2.49)-(2.53) for $\zeta \cdot n > 0$, where $\zeta = \zeta_y e_y$, characterized by the wall temperature ($\tau = \tau_w$), the wall velocity and the n_w parameter of Eq. (2.32), that can be obtained in terms of the reduced distribution functions as

$$n_w = - \frac{\int_{\zeta \cdot n < 0} (\zeta \cdot n) Y^- d\zeta_y}{\int_{\zeta \cdot n > 0} \frac{(\zeta \cdot n)}{(\pi\tau_w)^{1/2}} \exp\left[-\frac{\zeta_y^2}{\tau_w}\right] d\zeta_y} \quad (2.61)$$

The system of kinetic equations for the reduced distribution functions Eqs. (2.44)-(2.48) for the BGK model or Eqs. (2.55)-(2.59), coupled with the expressions for the macroscopic quantities Eqs. (2.60), under the boundary conditions given in terms of Eq. (2.61) are solved.

2.5.2 Projection on z component

In order to eliminate only the z component of the molecular velocity the following two reduced distribution functions need to be specified.

$$Y(y, \zeta_x, \zeta_y) = \int_{-\infty}^{+\infty} g(y, \zeta_x, \zeta_y, \zeta_z) d\zeta_z \quad (2.62)$$

and

$$\Phi(y, \zeta_x, \zeta_y) = \int_{-\infty}^{+\infty} \zeta_z^2 g(y, \zeta_x, \zeta_y, \zeta_z) d\zeta_z \quad (2.63)$$

In this case the kinetic equation is taken with the external acceleration term, and for the BGK model the system for the two reduced distribution functions becomes

$$\zeta_y \frac{\partial Y}{\partial y} + \bar{F} \frac{\partial Y}{\partial \zeta_x} = \delta_0 n \tau^{1-\omega} (Y^M - Y) \quad (2.64)$$

and

$$\zeta_y \frac{\partial \Phi}{\partial y} + \bar{F} \frac{\partial \Phi}{\partial \zeta_x} = \delta_0 n \tau^{1-\omega} (\Phi^M - \Phi) \quad (2.65)$$

while for the Shakhov model the system becomes

$$\zeta_y \frac{\partial Y}{\partial y} + \bar{F} \frac{\partial Y}{\partial \zeta_x} = \delta_0 n \tau^{1-\omega} \left(Y^M \left\{ 1 + \frac{4}{15} \frac{[q_x(\zeta_x - u_x) + q_y(\zeta_y - u_y)]}{n \tau^2} \left[\frac{(\zeta_x - u_x)^2 + (\zeta_y - u_y)^2}{\tau} - 2 \right] \right\} - Y \right) \quad (2.66)$$

and

$$\zeta_y \frac{\partial \Phi}{\partial y} + \bar{F} \frac{\partial \Phi}{\partial \zeta_x} = \delta_0 n \tau^{1-\omega} \left(\Phi^M \left\{ 1 + \frac{4}{15} \frac{[q_x(\zeta_x - u_x) + q_y(\zeta_y - u_y)]}{n \tau^2} \left[\frac{(\zeta_x - u_x)^2 + (\zeta_y - u_y)^2}{\tau} - 1 \right] \right\} - \Phi \right) \quad (2.67)$$

where the reduced Maxwellians are

$$Y^M = \frac{n}{\pi \tau} \exp \left(-\frac{(\zeta_x - u_x)^2 + (\zeta_y - u_y)^2}{\tau} \right) \quad (2.68)$$

and

$$\Phi^M = \frac{n}{2\pi} \exp \left(-\frac{(\zeta_x - u_x)^2 + (\zeta_y - u_y)^2}{\tau} \right) = Y^M \frac{\tau}{2} \quad (2.69)$$

The macroscopic quantities can be expressed in terms of those two reduced distribution functions in the following way

$$n(y) = \int_{-\infty}^{+\infty} \int_{-\infty}^{+\infty} Y d\zeta_x d\zeta_y \quad (2.70a)$$

$$u_x(y) = \frac{1}{n} \int_{-\infty}^{+\infty} \int_{-\infty}^{+\infty} \zeta_x Y d\zeta_x d\zeta_y \quad (2.70b)$$

$$u_y(y) = \frac{1}{n} \int_{-\infty}^{+\infty} \int_{-\infty}^{+\infty} \zeta_y Y d\zeta_x d\zeta_y \quad (2.70c)$$

$$\tau(y) = \frac{2}{3n} \int_{-\infty}^{+\infty} \int_{-\infty}^{+\infty} \left\{ [\zeta_x^2 + \zeta_y^2] Y + \Phi \right\} d\zeta_x d\zeta_y - \frac{2}{3} u_x^2 - \frac{2}{3} u_y^2 \quad (2.70d)$$

$$q_x(y) = \int_{-\infty}^{+\infty} \int_{-\infty}^{+\infty} \left[\left((\zeta_x - u_x)^2 + (\zeta_y - u_y)^2 \right) Y + \Phi \right] (\zeta_x - u_x) d\zeta_x d\zeta_y \quad (2.70e)$$

$$q_y(y) = \int_{-\infty}^{+\infty} \int_{-\infty}^{+\infty} \left[\left((\zeta_x - u_x)^2 + (\zeta_y - u_y)^2 \right) Y + \Phi \right] (\zeta_y - u_y) d\zeta_x d\zeta_y \quad (2.70f)$$

$$p_{xx}(y) = 2 \int_{-\infty}^{+\infty} \int_{-\infty}^{+\infty} (\zeta_x - u_x)^2 Y d\zeta_x d\zeta_y \quad (2.70g)$$

$$p_{yy}(y) = 2 \int_{-\infty}^{+\infty} \int_{-\infty}^{+\infty} (\zeta_y - u_y)^2 Y d\zeta_x d\zeta_y \quad (2.70h)$$

$$p_{xy}(y) = 2 \int_{-\infty}^{+\infty} \int_{-\infty}^{+\infty} (\zeta_x - u_x)(\zeta_y - u_y) Y d\zeta_x d\zeta_y \quad (2.70i)$$

$$p_{zz}(y) = 2 \int_{-\infty}^{+\infty} \int_{-\infty}^{+\infty} \Phi d\zeta_x d\zeta_y \quad (2.70j)$$

The outgoing distribution at the boundaries is of the form of the reduced Maxwellian distributions (2.68) and (2.69) characterized by the wall temperature and velocity and the n_w parameter is taken in terms of the reduced incoming distributions in the following way

$$n_w = - \frac{\int_{\zeta \cdot \mathbf{n} < 0} (\zeta \cdot \mathbf{n}) Y^-(r, \zeta) d\zeta_x d\zeta_y}{\int_{\zeta \cdot \mathbf{n} > 0} \frac{(\zeta \cdot \mathbf{n})}{\pi \tau_w} \exp \left[-\frac{(\zeta_x - u_{w,x})^2 + (\zeta_y - u_{w,y})^2}{\tau_w} \right] d\zeta_x d\zeta_y} \quad (2.71)$$

The system of kinetic equations for the reduced distribution functions Eqs. (2.64),(2.65) for the BGK model or Eqs. (2.66),(2.67), coupled with the expressions for the macroscopic quantities Eqs. (2.70), under the boundary conditions given in terms of Eq. (2.71) are solved.

3. Description and formulation of the method

3.1 Formulation of the non-linear BE

The non-linear Boltzmann equation is

$$\frac{\partial f}{\partial t} + \xi_x \frac{\partial f}{\partial x} + \xi_y \frac{\partial f}{\partial y} + \xi_z \frac{\partial f}{\partial z} + F_x \frac{\partial f}{\partial \xi_x} + F_y \frac{\partial f}{\partial \xi_y} + F_z \frac{\partial f}{\partial \xi_z} = Q \quad (3.1)$$

the left hand side of Eq. (3.1) is the streaming part, describing how the distribution function changes due to the free motion of particles due to their velocities and how it changes due to some external force field \mathbf{F} . We can group together the terms of the left hand side of Eq. (3.1) introducing the following two operators

$$\nabla_r = \frac{\partial}{\partial x} \mathbf{e}_x + \frac{\partial}{\partial y} \mathbf{e}_y + \frac{\partial}{\partial z} \mathbf{e}_z \quad (3.2)$$

and

$$\nabla_\xi = \frac{\partial}{\partial \xi_x} \mathbf{e}_{\xi_x} + \frac{\partial}{\partial \xi_y} \mathbf{e}_{\xi_y} + \frac{\partial}{\partial \xi_z} \mathbf{e}_{\xi_z} \quad (3.3)$$

Now Eq. (3.1) can be rewritten as

$$\frac{\partial f}{\partial t} + \boldsymbol{\xi} \cdot (\nabla_r f) + \mathbf{F} \cdot (\nabla_\xi f) = Q \quad (3.4)$$

the first term of the left hand side of Eq. (3.4) is the change of the distribution function with time, the second is the change due to free motion and the third the change due to external fields. The left hand side is essentially the material derivative of f , so we can replace it using the operator

$$\frac{D}{Dt} = \frac{\partial}{\partial t} + \boldsymbol{\xi} \cdot (\nabla_r) + \mathbf{F} \cdot (\nabla_\xi) \quad (3.5)$$

and Eq. (3.4) can now be written as

$$\frac{Df}{Dt} = Q \quad (3.6)$$

The right hand side of Eq. (3.1) denotes the change of f due to intermolecular collisions, and according to the Boltzmann equation it is given, for the general case, by a five-fold integral. This is exactly the reason why the direct solution of BE is a cumbersome and very demanding task. In order to simplify it we make use of the so-called kinetic models that provide much simpler expressions for the right hand side. For the formulation of the method we need to refer to only some properties they have. Kinetic models can be represented by

$$Q_{\text{mod}} = f^+ - f^- \quad (3.7)$$

where f^+, f^- are the “gain” and “loss” parts respectively, that is the particles entering a particular phase space element and the particles departing from it. It is typical for models to approach f^+ as a function of only macroscopic quantities, while f^- is a function of the distribution function of the phase space element that we are solving for. So the distribution function in the phase space element that we are solving for does not directly depend on the value of the distribution function at other phase space elements, but is only connected to them through the macroscopic quantities. This particular property makes it possible to decrease the computational effort and memory requirement for steady-state simulations and also to make the parallelization of the method easy and effective as only PM (particle-mesh) interaction is considered. This property will be used later in this chapter.

3.2 Basic description of the PIC method

In order to solve the problem using PIC methods, Eq. (3.6) is split into a system of equations that for a time step (k) can be represented in the form of the following two auxiliary problems

$$\frac{Df_1}{Dt} = 0, \quad f_1^{(k)} = f^{(k)} \quad (3.8a)$$

$$\frac{\partial f_2}{\partial t} = Q_{\text{mod}}, \quad f_2^{(k)} = f_1^{(\overline{k+1})} \quad (3.8b)$$

Using this splitting method, at each time step we solve problem (3.8a) with the initial condition $f_1^{(k)} = f^{(k)}$ and find the auxiliary solution $f_1^{(\overline{k+1})}$. The solution of problem (3.8a) gives us the new position and velocity of the particles of the initial distribution $f^{(k)}$. Then we use this solution $f_1^{(\overline{k+1})}$ as an initial condition for problem (3.8b) and find the new value of the distribution function after the collisions. The solution of problem (3.8b), $f_2^{(k+1)}$, is the distribution function at the end of the time step $f^{(k+1)}$. The solution is now found at two steps. The first step (3.8a) is a Lagrangian step, while the second step (3.8b) is an Eulerian step. Those steps are solved in a different way.

Solution of the Lagrangian step:

It is seen from (3.8a) that during the Lagrangian step the value of the distribution function does not change, the only change is in the position and velocity. In order to simulate this step, assuming a time step Δt , the laws of motion are used, essentially, following the

characteristics. For a case where external forces are absent ($\mathbf{F} = \mathbf{0}$), the initial (\mathbf{r}_i) and final (\mathbf{r}_f) position vectors are connected by

$$\mathbf{r}_f = \mathbf{r}_i + \boldsymbol{\xi} \Delta t \quad (3.9)$$

and the distribution function is transferred (without changing its value). In this step the application any discrete differencing techniques is avoided.

Solution of the Eulerian step:

For the solution of the Eulerian step, the value of the distribution function due to collisions is altered. The distribution function at the new location is altered through problem (3.8b). It is seen that in this step discrete differencing techniques have to be used. Using a first order approach the Eulerian step can be treated as

$$\frac{\partial f_2}{\partial t} = Q_{\text{mod}} \Rightarrow \frac{f_2^{(k+1)} - f_2^{(k)}}{\Delta t} \approx Q_{\text{mod}} \Rightarrow f_2^{(k+1)} \approx f_2^{(k)} + \Delta t Q_{\text{mod}} \quad (3.10)$$

It should also be noted that the Lagrangian step is conservative, but this is not ensured for the Eulerian step. During the simulation this has to be checked, and if needed a conservative scheme has to be used.

In the following sections the way this method is applied to several cases will be presented. Section 3.3 is dedicated to time dependent flows, 3.4 to force driven flows and finally the steady state solution method will be presented in section 3.5

3.3 Time dependent flows

Time dependency is inherent in this method, even if the steady state solution is desired. However, it is distinguished here from the steady state simulations, as for the latter some modifications and simplifications will be made, allowing us to reduce memory requirements and computational cost. For time dependent simulations it is required to know the value of the distribution function at each point of the phase space at all times. The simulation starts by generating simulator particles, according to the initial distribution at various points inside the flow field, typically several at each cell and for each molecular velocity. For this initial distribution of particles the velocities are assigned in a deterministic way. This process is repeated for all considered velocities and several particles are created for each velocity. The position inside the cells can be given either in a deterministic way (at given locations inside the cell) or in a stochastic way, at random points inside the cell. Either way the results of the simulation should not be altered drastically. The magnitude of the distribution carried by each

particle is determined by the initial distribution function, typically a Maxwellian distribution. For cases where more than one distribution functions have to be determined (reduced distributions, mixture flows, polyatomic gasses), two or more values can be assigned to each particle and then the Lagrangian step is not altered, while the Eulerian step is performed once for each of the distributions associated with the particle. This attribute, that one particle can carry more than one distributions cannot be applied when the Lagrangian step cannot be done only once, i.e. when the method is applied in a mixture flow with one electrically charged component and one neutral in the presence of an electric or magnetic field.

After the initial condition has been applied the simulation can start. At each time step several events have to take place.

- Step 1:* For each molecular velocity and for each boundary cell a simulator particle is created.
- Step 2:* The Lagrangian step is carried out according to Eq. (3.8a) for each simulator particle.
- Step 3:* The particles that have exited the flow field are determined and are moved at the boundary position.
- Step 4:* The Eulerian step is carried out according to Eq. (3.8b) for each simulator particle.
- Step 5:* For those particles that have exited the flow field in step 3, step 4 is altered to account for the portion of the time that they traveled outside of the flow field.
- Step 6:* For the particles that exited the flow field in step 3 and have been position on the boundary according to step 3, based on the new value determined at step 5, the integrals for the boundary condition parameters are determined and then they are deleted.
- Step 7:* For each cell, the value of the distribution function is determined by averaging the values of all simulator particles in this cell, for each velocity, and using this value the integrals for the macroscopic quantities are determined. Then we move to step 1 for the next time step.

One issue that has to be determined is the characteristic time. For the Lagrangian step the characteristic time is $\tau_L = L / v_0$, where L is a characteristic length and v_0 is the characteristic velocity, which is the mean thermal velocity. For the Eulerian step the characteristic time is τ_E that is of the order of the mean free time and the inverse of the collision frequency, that is $\tau_E = \lambda / v_0$, where λ is the mean free path. The ratio between those two characteristic times is $\tau_E / \tau_L = \lambda / L = Kn$ which is of the order of the Knudsen

number. So the two characteristic times can vary greatly, for very rarefied flows the Eulerian characteristic time is much larger than the Lagrangian and the opposite is the case for near continuum flows. For flows in the transition regime the two time intervals are close. In the simulations the Lagrangian characteristic time is used as the characteristic time.

3.4 Flows with external force fields

The simulation of flows with external fields by the direct simulation of Eq. (3.1) with the appropriate kinetic model is a difficult task. Using the currently described method this task becomes much easier. The Eulerian step is not affected and the only change has to be done in the Lagrangian step. Previously the solution of the Lagrangian step was described by Eq. (3.9) for cases without external fields. When an external force field is present the equations of motion have to include this external acceleration, so instead of Eq. (3.9) the following initial value problem has to be solved

$$\frac{d\mathbf{r}}{dt} = \boldsymbol{\xi} \quad (3.11a)$$

$$\frac{d\boldsymbol{\xi}}{dt} = \mathbf{F} \quad (3.11b)$$

so instead of just the position, the velocity is also updated. The values of position and velocity at the start of the time step are known $(\mathbf{r}(t), \boldsymbol{\xi}(t))$ and the values at the end of the time step are to be found $(\mathbf{r}(t+\Delta t), \boldsymbol{\xi}(t+\Delta t))$. Steps 6 and 7, where integrals of the distribution function have to be calculated, should also be changed. In step 7 the value of the distribution function at each cell is found by averaging the simulator particle values for each velocity. This value now has to be multiplied by the determinant of the Jacobian matrix, in order to use the same weighting factors. This Jacobian is

$$J = \begin{bmatrix} \frac{d\xi_x(t+\Delta t)}{d\xi_x(t)} & \frac{d\xi_x(t+\Delta t)}{d\xi_y(t)} & \frac{d\xi_x(t+\Delta t)}{d\xi_z(t)} \\ \frac{d\xi_y(t+\Delta t)}{d\xi_x(t)} & \frac{d\xi_y(t+\Delta t)}{d\xi_y(t)} & \frac{d\xi_y(t+\Delta t)}{d\xi_z(t)} \\ \frac{d\xi_z(t+\Delta t)}{d\xi_x(t)} & \frac{d\xi_z(t+\Delta t)}{d\xi_y(t)} & \frac{d\xi_z(t+\Delta t)}{d\xi_z(t)} \end{bmatrix} \quad (3.12)$$

or in a more compact form

$$J_{ij} = \frac{d\xi_i(t+\Delta t)}{d\xi_j(t)} \quad (3.13)$$

3.5 Steady state flows

When only the steady state solution is required several modifications can be made in order to reduce memory requirements and computational effort. It is not required to use the same time step for all particles. Different time steps can be used for each of the molecular velocities, in such a way that it is smaller than the cell transversal time (the time needed to cross one cell, with the given velocity), but since it is not needed to tune all particles in order to get the time evolution, it can be much larger for small velocities compared to large velocities. Another thing is that the initial condition does not have to be specified in terms of the initial distribution function and create a large number of particles that simulate the flow. It is sufficient to specify the initial conditions only at a macroscopic quantities level and then, instead of having a very big number of simulator particles, the evolution of one particle at a time can be studied. The simulation for the steady state flows can be summarized in the following pseudocode:

Step 1: Apply initial conditions.

Step 2: Store old values of macroscopic quantities.

Step 3: Iterate for every molecular velocity.

Step 4: Iterate for every boundary cell that has an outgoing distribution at the current molecular velocity.

Step 5: Repeatedly apply (3.8a) in order to find the new position and velocity and (3.8b) in order to find the new value of the distribution function until a boundary edge has been reached. During the application of (3.8) the values of the particle are averaged at its travel in a cell, and when it has exited the cell the partial sums of the macroscopic quantities integrals are calculated.

Step 6: When a boundary has been reached, the integrals for the boundary condition parameters are calculated.

Step 7: End of iteration for all boundary cells (4).

Step 8: End of iteration for all molecular velocities (3).

Step 9: Check for convergence and end the simulation or go to step 2.

3.6 PIC codes

In the framework of this thesis only some basic codes have been developed in order to check the applicability and accuracy of the method for rarefied gas flows. The main characteristics distinguishing the codes are the number of physical space coordinates and the number of molecular velocity coordinates. The codes are named as PmVn where m is the

number of physical space coordinates and n is the number of molecular velocity coordinates, so P1V2 is a code that solves flows that are dependent on one physical space direction and two molecular velocity directions. It should be noted that for all codes both the physical space and molecular velocity coordinate systems are Cartesian. Moreover, this simple four symbol name implies that the code simulates steady state flows.

All pic codes, during each time step, follow some basic steps that can be summarized as: move the simulator particle in the flow field using the laws of free motion (Lagrangian step), find the new cell that particle has traveled into, find the new value of the distribution (Eulerian step), calculate the partial sums of the integrals. The above steps are applied to all particles. Below, a brief description of the developed codes is given.

3.5.1 The P1V1 code

The P1V1 code is used to simulate problems where the distribution function depends on one physical space component (y) and one molecular velocity component (ζ_y), as can be seen in Figure 3.1. Since one molecular velocity component is taken into consideration, it is implied that the projection procedure described in section 2.5.1 on both ζ_x and ζ_z has been applied. This code simulates the flow solving the system of Eqs. (2.44)-(2.48) for the BGK and Eqs.(2.55)-(2.59) for the Shakhov model, under the boundary conditions specified in Eq. (2.61) and the macroscopic quantities are taken from Eqs. (2.60). This system of the integrodifferential equations for the reduced distribution functions is solved using the PIC method described in section 3.4.

In order to apply this method, the physical and molecular velocity spaces have to be discretized. The physical space is divided into N_l equally spaced cells of length $\Delta y = 1/N_l$, while the roots of a Legendere polynomial of order N_m , accordingly mapped from $(-1, +1)$ to $(-\infty, +\infty)$, are used as the discrete values of the molecular velocity.

The P1V1 algorithm is summarized in the flow chart of Figure 3.3, where the main aspects of the algorithm are shown. The initial conditions are applied at a macroscopic quantities level, and not as an initial distribution, then for each iteration of the method, the code iterates for all discrete values of the molecular velocity and depending on whether the velocity is positive or negative a particle is created at the bottom or top wall respectively. Then this particle is moved through the flow field and the values of the distribution functions it carries are constantly changed. During the motion inside a cell, at each time step, the values it carries are averaged and when it leaves the cell the partial sums of the macroscopic quantities are

calculated. When the particle reaches a boundary the partial sums of Eq. (2.61) are calculated and the next particle is created to repeat the process. When the iteration for all molecular velocities is finished, the macroscopic quantities are calculated using the partial sums and then a check for convergence is performed.

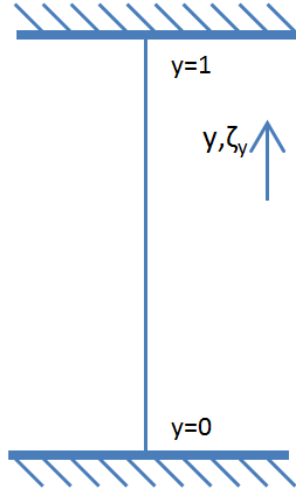


Figure 3.1: The geometry solved by P1V1.

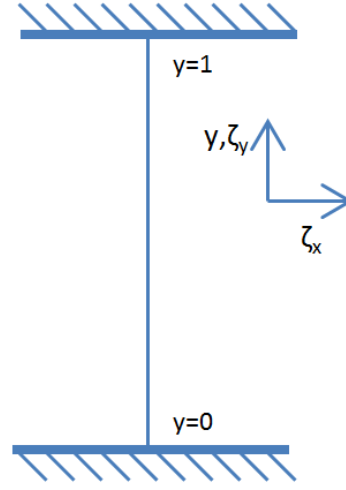


Figure 3.2: The geometry solved by P1V2.

3.5.2 The P1V2 code

The P1V2 algorithm simulates problems where the distribution functions depends on only one physical space direction (y) and two molecular velocity components (ζ_x) and (ζ_y) as is shown in Figure 3.2. The P1V2 code can simulate all the cases that can be solved by P1V1, but the opposite is not possible. Of course as P1V2 has one more independent variable than P1V1 the computational cost associated with it is much larger. The set of integrodifferential equations solved by P1V2 is Eqs. (2.64) and (2.65) for the BGK model and Eqs. (2.66) and (2.67) for the Shakhov model, under the boundary conditions given in terms of Eq. (2.71), while the macroscopic quantities are calculated for Eqs. (2.70).

The physical space discretization is the same as for P1V1. For the molecular velocity space, the same as in P1V1 discretization, using the roots of a Legendre polynomial is used for the y -direction of the molecular velocity space, but the x -direction is simply divided into equally spaced intervals. The reason for this is that an external acceleration in the x -direction acts on the particles. So particles departing from the boundary can be accelerated to very high velocities as they travel in the flow field, but the particles coming from collisions have relatively small velocities. In order to cover the whole range of molecular velocities, the upper and lower limits have to be adjusted as the external acceleration is changed and in order to achieve this, this kind of discretization has to be used.

The P1V2 algorithm is summarized in the flow chart of Figure 3.4. This algorithm is very similar to the P1V1 algorithm, with one significant difference. While for P1V1 has one component of the molecular velocity, P1V2 has two, so an additional iteration exists.

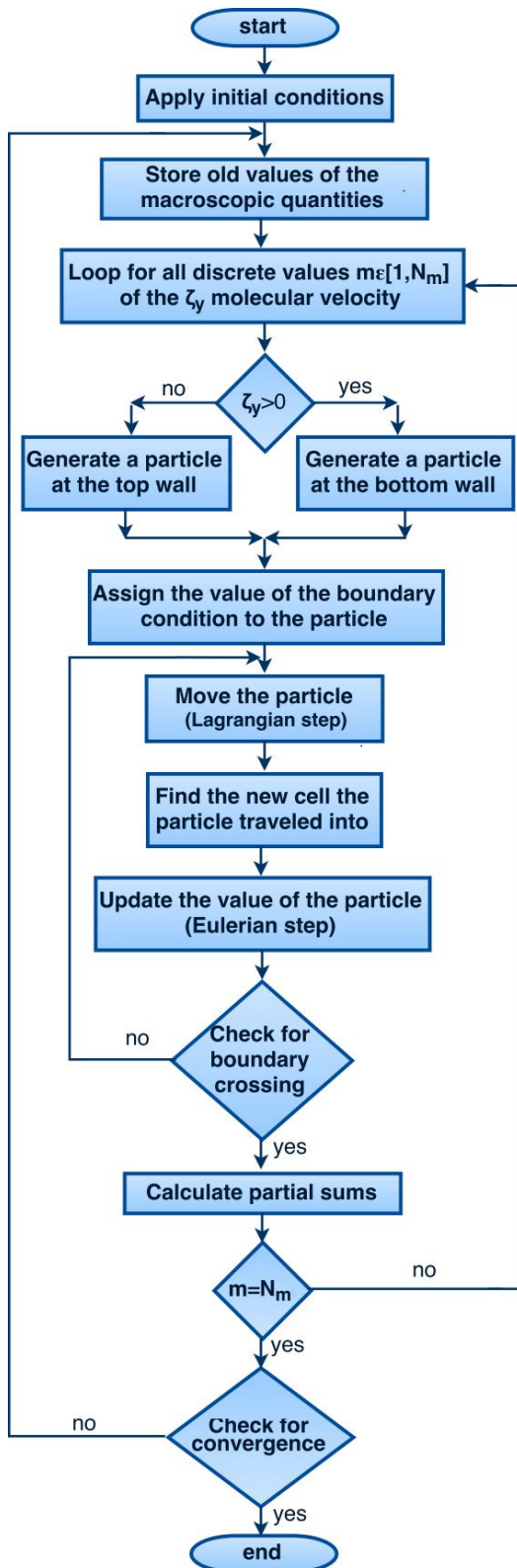


Figure 3.3: The P1V1 algorithm flow chart

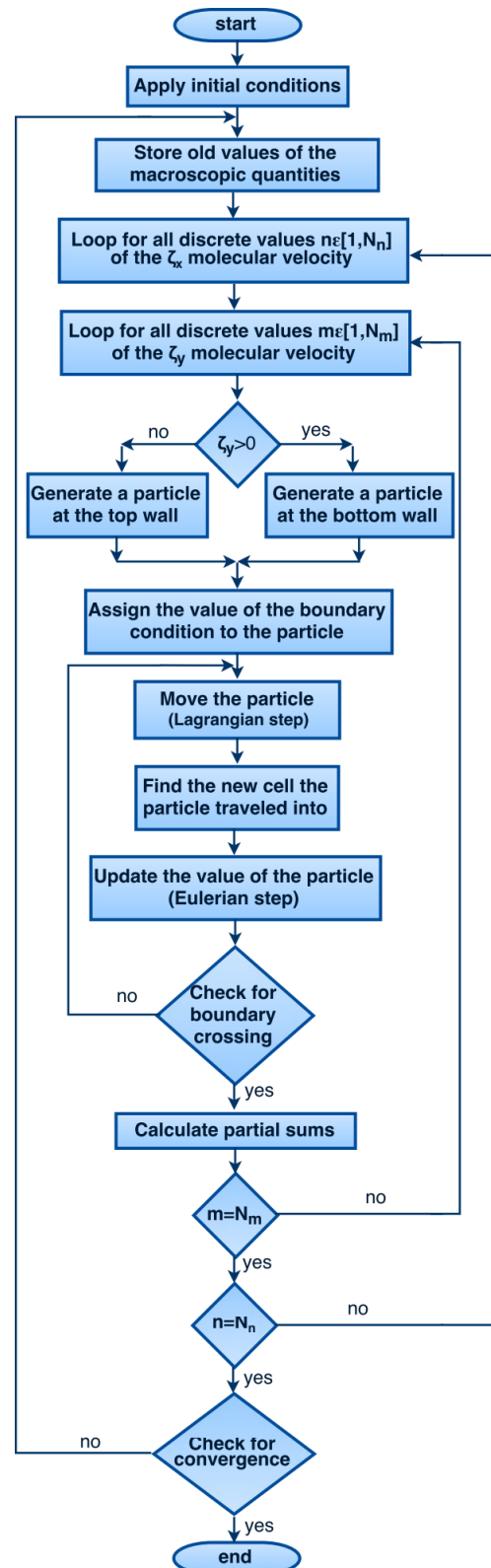


Figure 3.4: The P1V2 algorithm flow chart.

3.5.3 Extensions of P1V1 and P1V2 codes

In sections 3.5.1 and 3.5.2 two very simple cases of the described algorithm are realized, the P1V1 and P1V2. Those two simple codes are able to simulate rarefied gas flows with very good accuracy, as will be shown in the next chapters. Moreover, rarefied gas flows with external acceleration, a case hard to model using the conventional deterministic methods, has been simulated with considerable success. A potential future extension of this method is the P2V2 code, a code able to simulate two dimensional in the physical space problems, and since it is relatively easy to apply PIC methods to arbitrary geometries, a mesh independent code using the P2V2 algorithm could be created and even such a code using P3V3.

Another interesting field is axisymmetric rarefied gas flows, where an axisymmetric version of P1V2, the P1V2a, could be created simulating such flows. In this case, where the y -direction in the direction of the radius after the Lagrangian step, the particle has moved for the old position $(0, y_{old})$ to the new position $(dx, y_{old} + dy)$ it should be relocated to $(0, y_{new})$ so that it is on the radial direction Figure 3.5. Of course after the relocation of the particle the molecular velocity vector should also be rotated. It is noted that this way of solving axisymmetric flows may potentially offer advantages compared to the typical deterministic methods as this way the modeling of the free motion is closer to the real physical problem as the value of the distribution function is not altered in order to account for the symmetry but the position and molecular velocity are. Another advantage is that this way the discontinuities associated with the curvature at the convex boundary are not present.

A final potential extension, which however is not compatible with the simplifications for the steady state flows mentioned above, is the solution of the BE without substituting the collision integral with kinetic models. The using purely deterministic methods is hard and computationally demanding, due to the five-fold solution of the BE using stochastic methods (DSMC) is not a very hard task, but the solution collision integral. If however, the scheme remains deterministic, but the collision integral is calculated in a stochastic manner, (Monte Carlo integration) then the complexity of the simulation would be significantly lower, the solution would still be obtained in a deterministic manner (small statistical noise) and the exact BE would be solved, instead of a kinetic model.

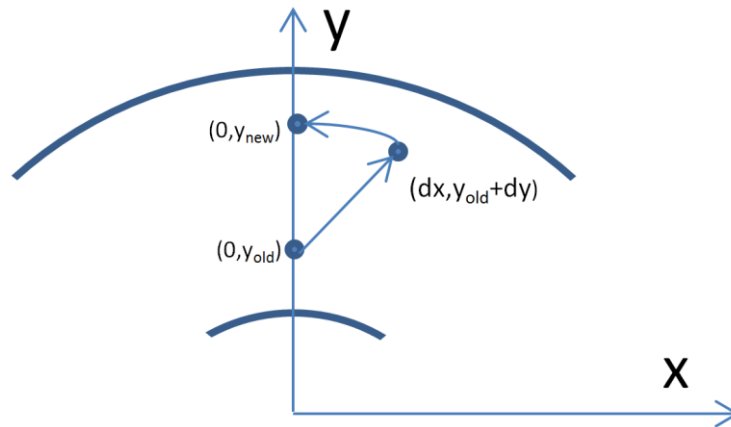


Figure 3.5: The Lagrangian step for axisymmetric flows.

3.6 Advantages of PIC codes

As can be seen from the above PIC codes offer some advantages, compared to typical discrete difference or elements methods. One of the main advantages is that PIC methods are easy to program and implement, as is the case for the described codes. Computationally expensive solution of linear systems is not required for the simulation. A great advantage comes from the way the Lagrangian step is solved, based on the laws of free motion. This makes the simulation of force driven flows and the simulation of complex geometries easy. Usually, PIC codes are hard to parallelize, but due to the property of the kinetic models discussed in section 3.1, this obstacle can be overcome, and in fact the PIC codes described above can be parallelized in a very straightforward manner. One disadvantage is that they usually require larger computational time than the alternatives. In typical deterministic algorithms, the travel from one node to the next is done in one step, but in PIC codes several steps are required. However, with the use of parallel computing this can be overcome.

4. Flow configuration and basic parameters of prototype problems

In this chapter the formulation of the benchmark problems, solved to test the accuracy of the developed methodology is presented. Three problems were chosen as test cases, the non-linear Couette flow and non-linear Fourier flow between parallel plates, which are solved using the P1V1 algorithm and the non-linear force driven Poiseuille flow between parallel plates solved using the P1V2 algorithm. The first two cases have also been solved using the P1V2 algorithm, but the results presented were obtained using the P1V1.

4.1 Non-linear Couette flow

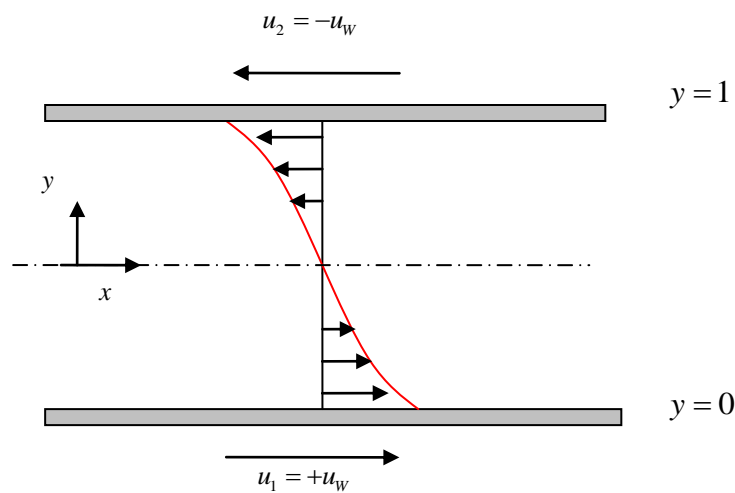


Figure 4.1: The Couette flow configuration.

The plane Couette flow is one of the traditional problems of fluid mechanics. The geometric configuration, shown in Figure 4.1, is relatively simple. Two infinitely long parallel plates are kept at a distance L , while a rarefied monatomic gas is confined between them. Initially the plates are still and the gas is at pressure P_0 and temperature T_0 , while the gas is at rest. Then the plates start moving in opposing directions with velocity of magnitude U_w and due to this motion of the plates a symmetric velocity profile is formed and due to compressibility a parabolic temperature profile is also developed. This flow is called pure shear flow, as the shear stress has a constant value at all points of the flow domain. After an appropriate amount of time, a steady state is reached and our objective is to find this steady state solution.

The problem is characterized by two parameters, the dimensionless magnitude of the wall velocity

$$u_w = U_w / \nu_0 \quad (4.1)$$

and the reference rarefaction parameter

$$\delta_0 = \frac{P_0 L}{\mu_0 \nu_0} \quad (4.2)$$

The molecular interaction model is chosen to be Hard Spheres, leading to $\omega = 0.5$, while the BGK model is used. The problem is solved for a wide range of the reference rarefaction parameter $\delta_0 \in [0, 10]$ ranging from the free molecular to near continuum regimes and for a wide range of the velocity magnitude $u_w \in [0.1, 2]$ and the shear stress is used in order to benchmark the accuracy of the results. The P1V1 algorithm will be used for this case.

4.2 Non-linear Fourier flow

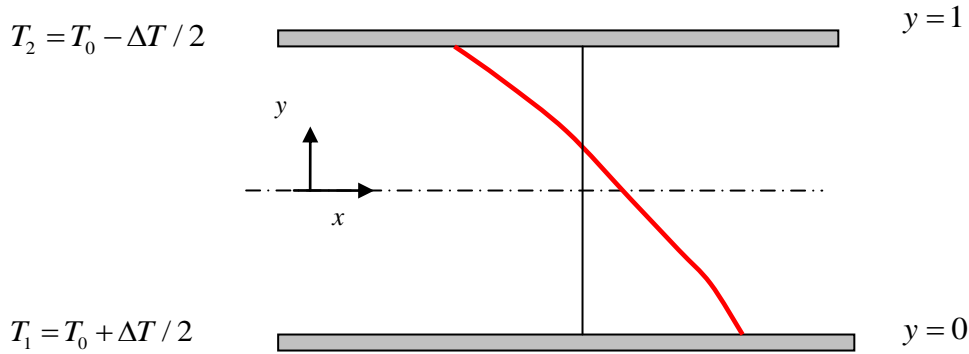


Figure 4.2: The Fourier flow configuration.

This problem is pure heat transfer, meaning there is no gas flow. The geometric configuration, shown in Figure 4.2, is very close to that of the Couette flow, however the boundaries here are still and are maintained at different temperatures T_1 and T_2 . Initially the gas is at a uniform temperature $T_0 = (T_1 + T_2)/2$ and then, due to the temperature difference of the two walls, a temperature profile is formed as well as a constant heat flux in the y direction. The parameters characterizing the problem are the reference rarefaction parameter

$$\delta_0 = \frac{P_0 L}{\mu_0 \nu_0} \quad (4.3)$$

and the dimensionless temperature difference

$$\beta = \frac{\Delta T}{2T_0} \quad (4.4)$$

The molecular interaction model is again chosen to be the Hard Sphere model, while simulation is based on the Shakhov kinetic model. A large range of the reference rarefaction parameter $\delta_0 \in [0,10]$ as well as three values of the dimensionless temperature difference $\beta = 0.1, 0.5$ and 0.9 corresponding to small, medium and large temperature differences is simulated. The constant heat flux in the y direction was used in order to benchmark the accuracy of the results. The P1V1 algorithm will be used for this case.

4.3 Non-linear Poiseuille flow

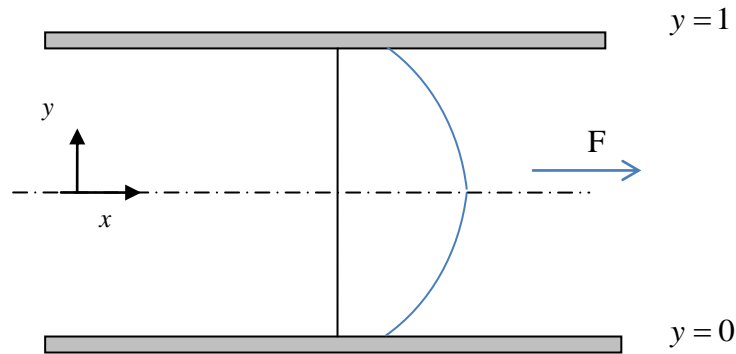


Figure 4.3: The Poiseuille flow configuration.

A more advanced benchmark problem is that of the force driven Poiseuille flow, shown in Figure 4.3. A monatomic rarefied gas is confined between two infinite parallel plates, the boundaries are kept still and have the same temperature. Initially the gas is at rest, with pressure P_0 and temperature T_0 . Then a uniform and constant external acceleration starts acting on the gas molecules in the x direction, setting the gas in motion. The parameters characterizing the flow are the reference Knudsen number

$$Kn_0 = \frac{2}{\sqrt{\pi}} \frac{\mu_0 \nu_0}{P_0 L} \quad (4.5)$$

and the magnitude of the dimensionless external acceleration F . The reference Knudsen number is connected to the reference rarefaction parameter as

$$\delta_0 = \frac{2}{\sqrt{\pi}} \frac{1}{Kn_0} \quad (4.6)$$

According to the definition of the rarefaction parameter given in the previous chapters the expression connecting it with the Knudsen number should be $\delta_0 = \frac{\sqrt{\pi}}{2} \frac{1}{Kn_0}$, however, in

order to make the comparison with published results easier, the definition of the Knudsen number given in [34] was used for this problem. In this problem the BGK model was used, with Maxwell molecules, $\omega=1$, while simulations were conducted for $Kn_0 = 0.1, 1$ and 10 covering the whole transition regime and for $F = 0.05$ and 0.5 corresponding to small and large external accelerations respectively. In order to benchmark the results, the normalized flow rate

$$M = \int_0^{0.5} n u_x dy = \int_{0.5}^1 n u_x dy \quad (4.7)$$

was used. The P1V2 algorithm will be used for this case.

4.4 Free molecular solutions

For the Couette and Fourier flows between parallel plates, closed analytical solutions in the free molecular regime can be derived, while for the Poiseuille problem as described in section 4.3 it is not possible to obtain free molecular solutions. For the Couette flow the free molecular values of the shear stress are used for comparison purposes, while for the Fourier flow, the values of the heat flux are used.

In order to obtain the analytical solution in the free molecular regime for the Couette flow, the kinetic equation is written as

$$\zeta_y \frac{\partial g}{\partial y} = 0 \quad (4.8)$$

and distinguishing for positive and negative velocities we get

$$g = \begin{cases} g_1, & \zeta_y > 0 \\ g_2, & \zeta_y < 0 \end{cases} \quad (4.9)$$

and due to the boundary conditions we have

$$g_1 = \frac{n_1}{\pi^{3/2}} \exp \left[-\zeta_x^2 - (\zeta_y - u_w)^2 - \zeta_z^2 \right] \quad (4.10)$$

$$g_2 = \frac{n_2}{\pi^{3/2}} \exp \left[-\zeta_x^2 - (\zeta_y + u_w)^2 - \zeta_z^2 \right] \quad (4.11)$$

Applying the impermeability condition at the bottom wall we have

$$u_y(0) = 0 \Rightarrow \int_{R^3} \zeta_y g d\zeta = 0 \Rightarrow \int_{-\infty}^{\infty} \int_0^{\infty} \int_{-\infty}^{\infty} \zeta_y g_1 d\zeta_x d\zeta_y d\zeta_z + \int_{-\infty}^{\infty} \int_{-\infty}^0 \int_{-\infty}^{\infty} \zeta_y g_2 d\zeta_x d\zeta_y d\zeta_z = 0 \Rightarrow$$

$$n_1 = n_2 \quad (4.12)$$

Moreover the density profile is

$$n^{fm} = \int_{R^3} g d\zeta = \int_{-\infty}^{\infty} \int_0^{\infty} \int_{-\infty}^{\infty} g_1 d\zeta_x d\zeta_y d\zeta_z + \int_{-\infty}^{\infty} \int_{-\infty}^0 \int_{-\infty}^{\infty} g_2 d\zeta_x d\zeta_y d\zeta_z = \frac{n_1}{2} + \frac{n_2}{2} \quad (4.13)$$

and since the average number density is unity

$$1 = \int_0^1 n^{fm} dy \Rightarrow \frac{n_1}{2} + \frac{n_2}{2} = 1 \quad (4.14)$$

and combining Eqs.(4.12) and (4.14) we get

$$n_1 = n_2 = 1 \quad (4.15)$$

The shear stress is now calculated as

$$p_{xy}^{fm} = 2 \int_{R^3} \zeta_x \zeta_y g d\zeta = 2 \int_{-\infty}^{\infty} \int_0^{\infty} \int_{-\infty}^{\infty} \zeta_x \zeta_y g_1 d\zeta_x d\zeta_y d\zeta_z + 2 \int_{-\infty}^{\infty} \int_{-\infty}^0 \int_{-\infty}^{\infty} \zeta_x \zeta_y g_2 d\zeta_x d\zeta_y d\zeta_z = 2 \frac{u_w}{\sqrt{\pi}} \quad (4.16)$$

The numerical results obtained using the developed algorithm for the free molecular cases will be compared to the results of Eq.(4.16).

For the Fourier flow, the kinetic equation is again Eq. (4.8) and for positive and negative velocities we get Eq. (4.9), but for the two different cases we now have

$$g_1 = \frac{n_1}{[\pi(1+\beta)]^{3/2}} \exp\left[-\frac{\zeta_x^2 + \zeta_y^2 + \zeta_z^2}{1+\beta}\right] \quad (4.17)$$

$$g_2 = \frac{n_2}{[\pi(1-\beta)]^{3/2}} \exp\left[-\frac{\zeta_x^2 + \zeta_y^2 + \zeta_z^2}{1-\beta}\right] \quad (4.18)$$

Applying the impermeability condition we now get

$$n_1 \sqrt{1+\beta} = n_2 \sqrt{1-\beta} \quad (4.19)$$

and for the average number density we have

$$\frac{n_1}{2} + \frac{n_2}{2} = 1 \quad (4.20)$$

and combining Eqs.(4.19) and (4.20) we get

$$n_1 = 2 \frac{\sqrt{1-\beta}}{\sqrt{1-\beta} + \sqrt{1+\beta}} \quad (4.21)$$

and

$$n_2 = 2 \frac{\sqrt{1+\beta}}{\sqrt{1-\beta} + \sqrt{1+\beta}} \quad (4.22)$$

For the heat flux we get

$$q_y^{fm} = \int_{R^3} \zeta^2 \zeta_y g d\zeta = \int_{-\infty}^{\infty} \int_0^{\infty} \int_{-\infty}^{\infty} \zeta^2 \zeta_y g_1 d\zeta_x d\zeta_y d\zeta_z + \int_{-\infty}^{\infty} \int_{-\infty}^0 \int_{-\infty}^{\infty} \zeta^2 \zeta_y g_2 d\zeta_x d\zeta_y d\zeta_z \Rightarrow$$

$$q_y^{fm} = \frac{4}{\sqrt{\pi}} \frac{\beta \sqrt{1-\beta} \sqrt{1+\beta}}{\sqrt{1+\beta} + \sqrt{1-\beta}} \quad (4.23)$$

The numerical results obtained using the developed algorithm for the free molecular cases will be compared to the results of Eq.(4.23).

5. Results and discussion

In this chapter results are presented for the three benchmark problems presented in chapter 4. The results presented are not very extensive, as all three of these problems have been extensively studied in the literature and our objective here is to test the accuracy of the presented algorithm. Comparison is performed with published results, as well as the analytical results for the free molecular regime derived in section 4.4.

5.1 Non-linear Couette flow

The first problem is that of the plane non-linear Couette flow, between two parallel plates, described in section 4.1. Simulations were conducted using the P1V1 code for a range of reference rarefaction parameters $\delta_0 \in [0, 10]$ and for various values of the wall velocity $u_w \in [0.1, 2]$. The BGK kinetic model was used, and the molecular interaction model was the Hard Spheres. For the molecular velocity discretization, the roots of the Legendre polynomial of order 80 were used, while the physical space was divided into 1.5×10^4 equally spaced intervals. The simulation ended when a convergence criteria of the form

$$\max_i \left\{ \left| n_i^{(k)} - n_i^{(k-1)} \right| + \left| u_{x,i}^{(k)} - u_{x,i}^{(k-1)} \right| + \left| \tau_i^{(k)} - \tau_i^{(k-1)} \right| \right\} < 10^{-6} \quad (5.1)$$

was met.

The shear stress for all cases simulated is shown in Table 5.1, which is constant along the flow domain. We observe that as the dimensionless wall velocity increases, the shear stress increases, while as the reference rarefaction parameter is increased the shear stress decreases. The velocity profiles for various values of the reference rarefaction parameter and wall velocity are shown in Figure 5.1. It is seen that for small values of δ_0 near the boundaries the slope of the velocity is not constant, although the shear stress is constant. This is natural for non-equilibrium flows, as the Newton law fails in such cases. Moreover, the failure of the no-slip boundary conditions is also observed. What is even more interesting is that for $\delta_0 = 0$, although the macroscopic velocity is zero, the shear stress has non-zero values. The temperature profiles for a range of the reference rarefaction parameter and wall velocity values are presented in Figure 5.2. Due to compressibility effects, a non-uniform temperature profile is formed, having a maximum at the middle of the flow domain. For small values of the wall velocity, when the flow is almost linear, the temperature does not depart a lot from the equilibrium temperature, but for fast flows due to non-linear phenomena the temperature increases greatly. Finally, as the degree of rarefaction increases, the temperature profile

becomes flat. The distributions of velocity and temperature have also been compared with results of [35], and are in good agreement.

The analytical free molecular results for the shear stress given by Eq. (4.16) are shown in Table 5.2. We observe that there is very good agreement with the numerical results shown in Table 5.1. The shear stress results for larger values δ_0 were compared to the results of [35] shown in Table 5.3 and the relative error was less than 0.04% , giving a very good agreement. It is noted that in order to compare the current results for the shear stress with those of [35], the values of Table 5.3 have been multiplied by the factor (-2) , due to the different conventions used. This problem was also simulated using the P1V2 algorithm, for limited cases, and those results were also in very good agreement with [35], however here only the results of P1V1 are shown.

5.2 Non-linear Fourier flow

The results for the heat transfer between parallel plates problem described in chapter (4.2) are presented here. Simulations were conducted using the P1V1 algorithm, with the Shakhov model and Hard Sphere molecules. Simulations were conducted for $\delta_0 \in [0,10]$ and $\beta = 0.1, 0.5$ and 0.9 , corresponding to small, medium and large temperature differences. For the molecular velocity space discretization the roots of the Legendre polynomial of order 80 were used, and the physical space was divided into 1.5×10^3 equally spaced intervals for small values of δ_0 and into 5×10^3 for larger. The simulation ended when a convergence criteria of the form

$$\max_i \left\{ \left| n_i^{(k)} - n_i^{(k-1)} \right| + \left| \tau_i^{(k)} - \tau_i^{(k-1)} \right| + \left| q_{y,i}^{(k)} - q_{y,i}^{(k-1)} \right| \right\} < 10^{-6} \quad (5.2)$$

was met.

The heat flux shown in Table 5.4 is constant along the flow domain and as expected the value of the heat flux increases as β increases, but decreases as δ_0 is increased for small temperature differences. For large temperature differences, the heat flux exhibits a non-monotonic behavior with respect to β , something that has been reported in the literature. The temperature profiles, for various values of δ_0 and the three simulated values of β are shown in Figure 5.3. We observe the temperature jump at the boundaries and that the slope of the temperature is not constant. Moreover, for $\delta_0 = 0$, while the temperature is constant, a heat flux exists. In Figure 5.4 the density profiles are presented. The density is inversely

proportional to the temperature, lower at the hot plate and higher at the cold one. The distributions of temperature and density are in good agreement with [36].

In Table 5.5 the free molecular results for the heat flux are presented, which are in very good agreement with the numerical results of Table 5.4. The numerical results for larger values of δ_0 were compared to the results of [36] shown in Table 5.6 and the relative difference was less than 0.08% giving a very good agreement. This problem was also simulated with the P1V2 algorithm, but here only the results of P1V1 are presented.

5.3 Poiseuille flow

The third benchmark problem, described in chapter 4.3, is the force driven Poiseuille flow between parallel plates. Simulations were conducted using the P1V2 algorithm, with the BGK model and Maxwell molecules, for small ($F = 0.05$) and large ($F = 0.5$) values of the external acceleration magnitude and covering the whole transition regime $Kn_0 = 0.1, 1$ and 10 . The small value of the external acceleration corresponds to close to linear flow, while the large one to non-linear flow. For the molecular velocity space discretization the roots of the simple polynomial of order 16 were used in the y direction, while the velocity space in the x direction was divided into 4×10^3 equally spaced intervals. The physical space was also divided into 4×10^3 intervals. The simulation ended when a convergence criteria of the form

$$\max_i \left\{ \left| n_i^{(k)} - n_i^{(k-1)} \right| + \left| u_{x,i}^{(k)} - u_{x,i}^{(k-1)} \right| + \left| \tau_i^{(k)} - \tau_i^{(k-1)} \right| \right\} < 10^{-6} \quad (5.3)$$

was met.

The dimensionless mass flow rate defined in Eq. (4.7) is shown in Table 5.7, for all cases simulated. As expected, as the magnitude of the external force increases, the mass flow rate also increases, but the behavior with respect to the reference Knudsen number is not monotonic, as the mass flow rate has a minimum value inside the transitional regime, known as the Knudsen minimum. The results of Table (5.7) were compared with results of [34] shown in Table 5.8 and the relative difference is less than 0.8%. This difference can be tolerated, especially considering that solving this problem using the typical deterministic schemes is very hard. In Figure 5.5 the velocity profiles for the cases simulated are shown, which are in good agreement with [34].

Table 5.1: Shear stress for the Couette flow, current work.

u_w	δ_0					
	0	0.001	0.01	0.1	1	10
0.1	1.1284(-1)	1.1274(-1)	1.1187(-1)	1.0449(-1)	6.7830(-2)	1.6638(-2)
0.5	5.6419(-1)	5.6382(-1)	5.6006(-1)	5.2510(-1)	3.4468(-1)	8.6132(-2)
0.9	1.0156	1.0153	1.0106	9.5482(-1)	6.4114(-1)	1.6635(-1)
1.1	1.2412	1.2413	1.2371	1.1743	7.9982(-1)	2.1236(-1)
1.5	1.6926	1.6937	1.6927	1.6231	1.1413	3.1862(-1)
2	2.2568	2.2602	2.2672	2.2028	1.6165	4.8082(-1)

Table 5.2: The analytical free molecular values of shear stress.

u_w	0.1	0.5	0.9	1.1	1.5	2
p_{xy}^{fm}	1.1284(-1)	5.6419(-1)	1.0155	1.2412	1.6926	2.2568

Table 5.3: Shear stress of the Couette flow [35].

u_w	δ_0			
	0	0.1	1	10
0.1	1.128(-1)	1.044(-1)	6.78(-2)	1.66(-2)
0.5	5.642(-1)	5.25(-1)	3.446(-1)	8.62(-2)

Table 5.4: Heat flux for the Fourier flow, current work..

β	δ_0				
	0	0.01	0.1	1	10
0.1	1.124(-1)	1.117(-1)	1.067(-1)	7.981(-2)	2.696(-2)
0.5	5.058(-1)	5.037(-1)	4.839(-1)	3.700(-1)	1.307(-2)
0.9	5.224(-1)	5.260(-1)	5.266(-1)	4.675(-1)	2.096(-1)

Table 5.5: The free molecular values of the heat flux.

β	q_y^{fm}
0.1	1.124(-1)
0.5	5.058(-1)
0.9	5.224(-1)

Table 5.6: Heat flux for the Fourier flow [36].

β	δ_0				
	0	0.01	0.1	1	10
0.1	1.124(-1)	1.117(-1)	1.067(-1)	7.981(-2)	2.694(-2)
0.5	5.058(-1)	5.037(-1)	4.839(-1)	3.700(-1)	1.307(-1)
0.9	5.224(-1)	5.260(-1)	5.266(-1)	4.675(-1)	2.096(-1)

Table 5.7: Normalized flow rate for the Poiseuille flow, current work.

	F	
Kn_0	0.05	0.5
0.1	7.419(-2)	5.319(-1)
1	3.848(-2)	3.498(-1)
10	4.972(-2)	4.397(-1)

Table 5.8: Normalized flow rate for the Poiseuille flow, [34].

	F	
Kn_0	0.05	0.5
0.1	7.374(-2)	5.280(-1)
1	3.841(-2)	3.492(-1)
10	4.961(-2)	4.400(-1)

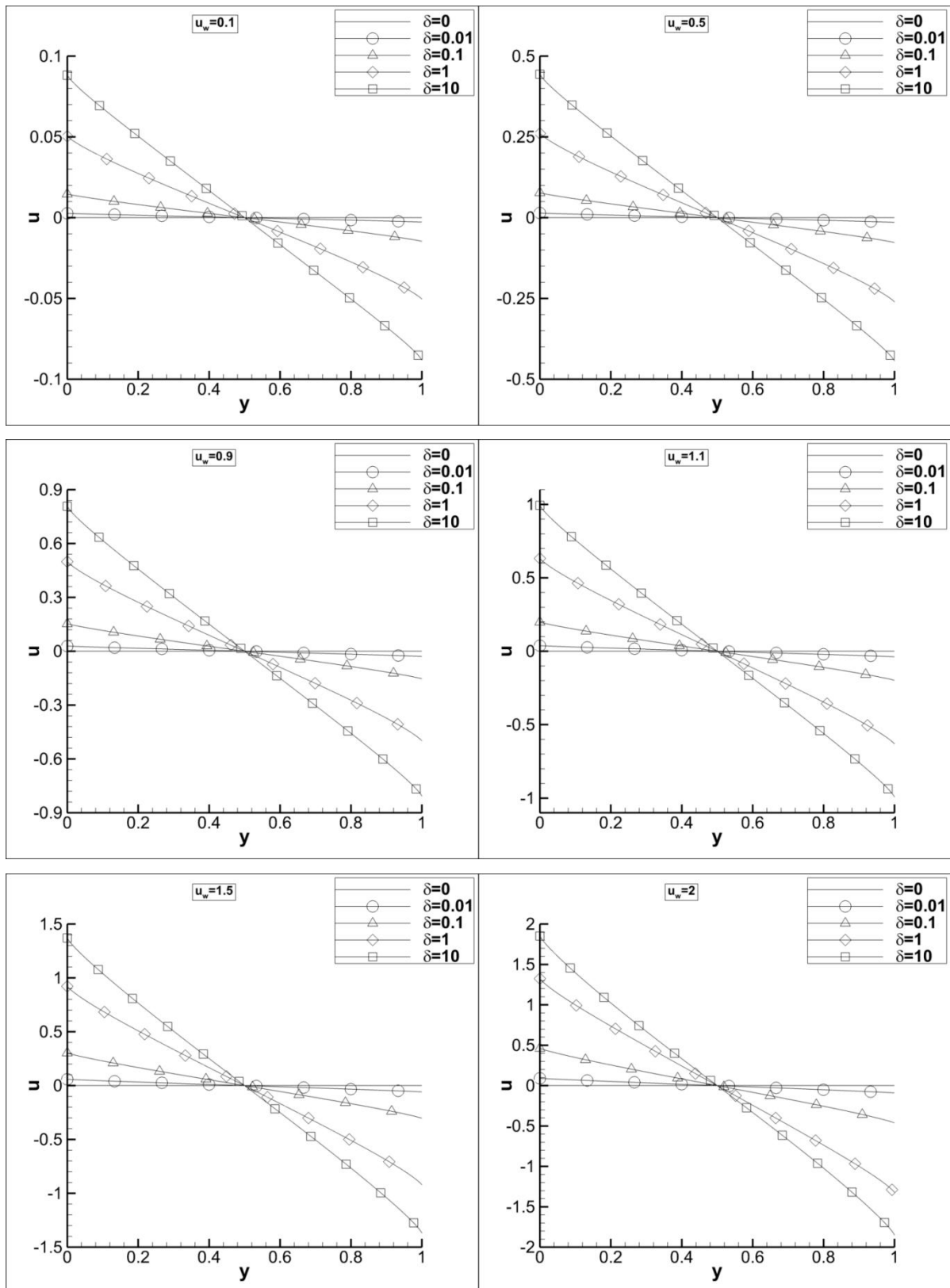


Figure 5.1: Velocity profiles for $u_w = 0.1, 0.5, 0.9, 1.1, 1.5$ and 2 and for $\delta_0 = 0, 0.01, 0.1, 1$ and 10 , for the Couette flow.

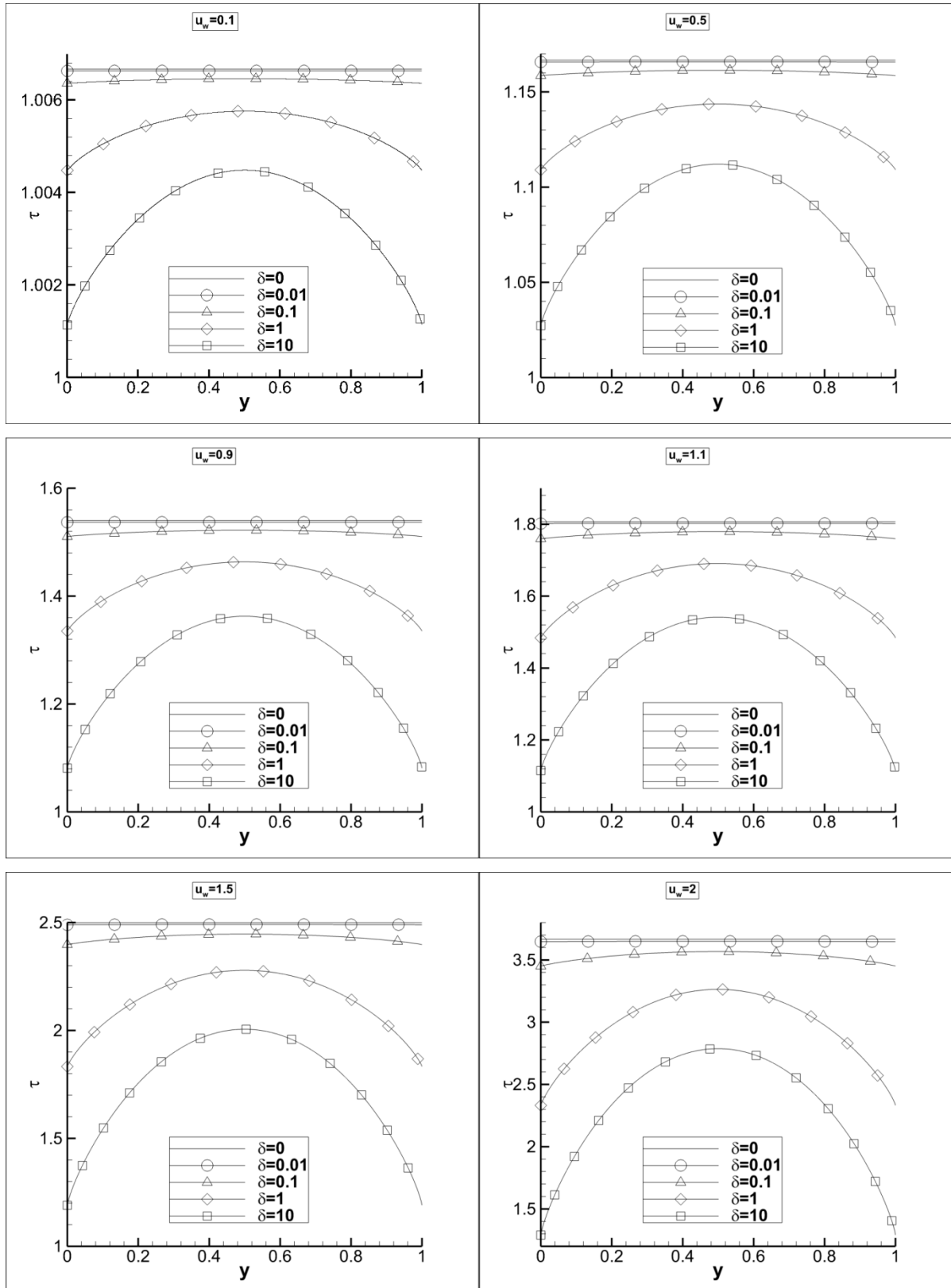


Figure 5.2: Temperature profiles for $u_w = 0.1, 0.5, 0.9, 1.1, 1.5$ and 2 and for $\delta_0 = 0, 0.01, 0.1, 1$ and 10 , for the Couette flow.

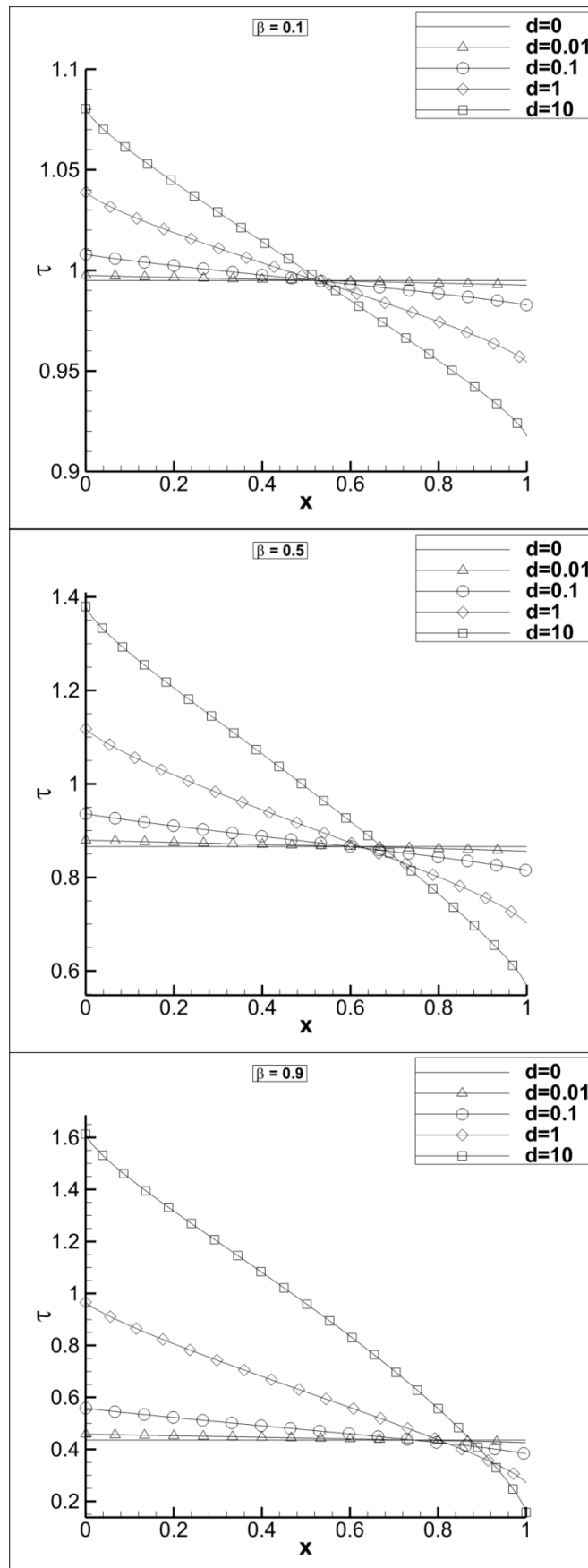


Figure 5.3: Temperature profiles for $\beta = 0.1, 0.5$ and 0.9 and $\delta_0 = 0, 0.01, 0.1, 1$ and 10 , for the Fourier flow.

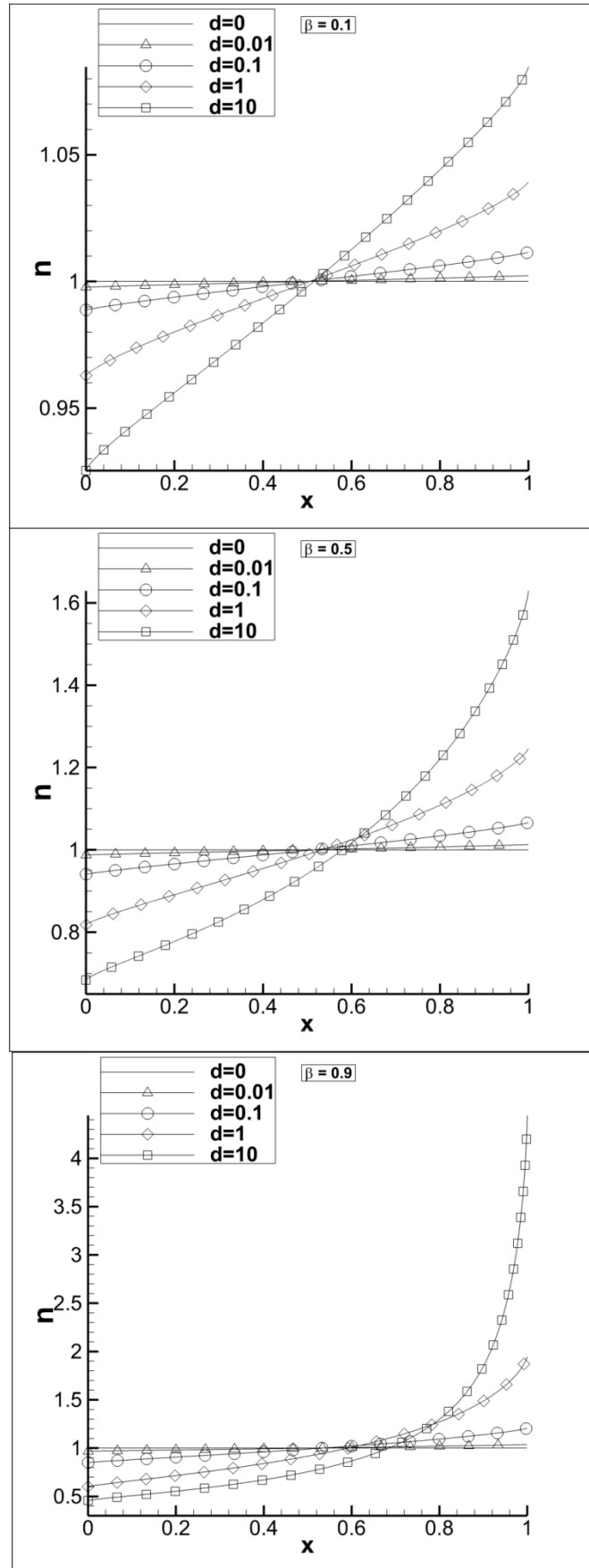


Figure 5.4: Density profiles for $\beta = 0.1, 0.5$ and 0.9 and $\delta_0 = 0, 0.01, 0.1, 1$ and 10 , for the Fourier flow.

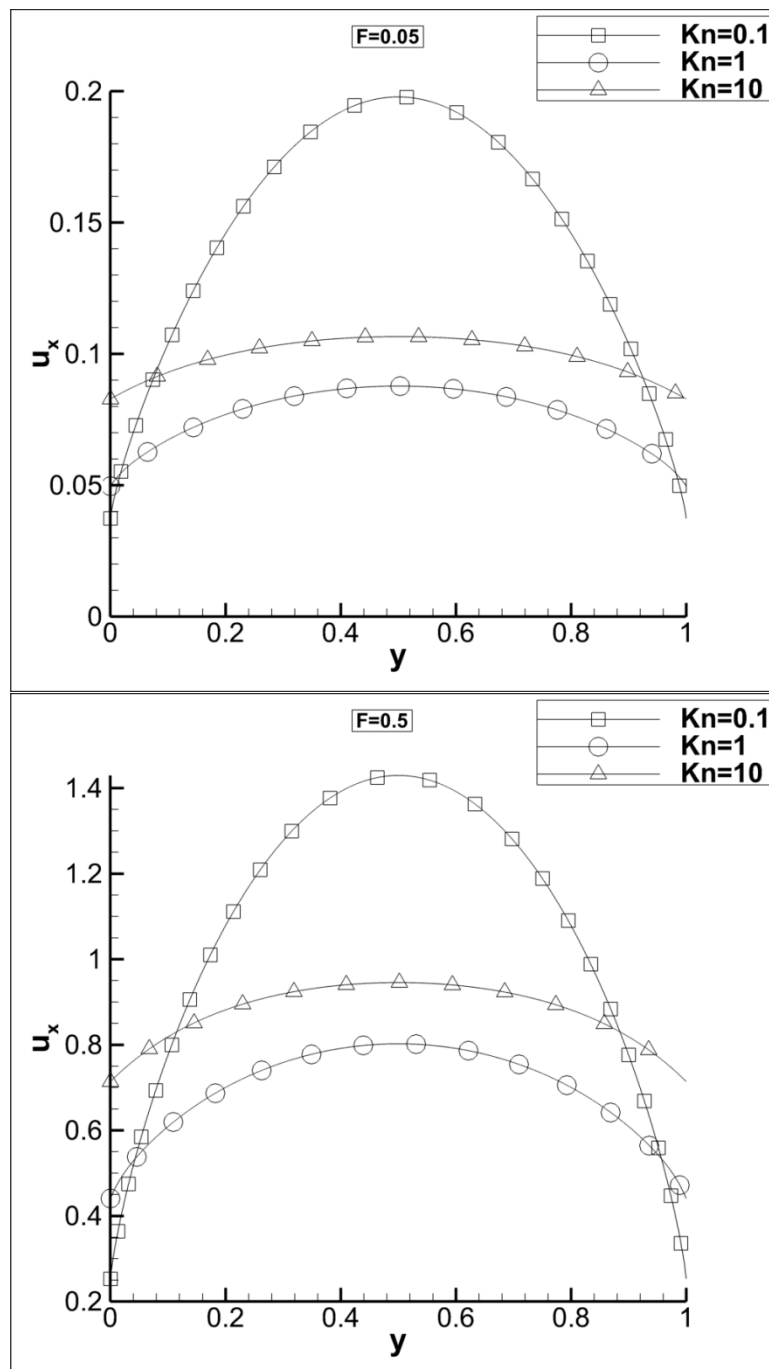


Figure 5.5: Velocity profiles for $F = 0.05$ and 0.5 and $Kn_0 = 0.1, 1$ and 10 , for the Poiseuille flow.

6. Concluding remarks

Rarefied gas dynamics is a very active field of research, driven by the need for accurate modeling and simulation in a number of fields, including vacuum technology, micro/nano-electromechanical systems and microfluidics. Currently, the two leading methods for flow simulation are the deterministic solution of the Boltzmann equation with the appropriate kinetic models and the stochastic simulation using the DSMC method. The deterministic methods, although very accurate have proven to be problematic to apply to complex geometries or for complicated particle interaction, cases where the DSMC method is widely used.

In the present work an introductory study on the application of particle-in-cell methods for deterministic simulation of rarefied gas flows is performed. Particle-in-cell methods have proven to be very effective and successful for the simulation of otherwise very demanding problems in the past and their application for rarefied flows is an interesting subject. In the context of this work, the basic aspects of Particle in Cell (PIC) codes for such flows are given and some basic algorithms are created. The algorithms developed are able to simulate compressible flows that depend on one physical space direction and one or two molecular velocity directions.

In order to test the accuracy of the method three prototype problems were used, the compressible plane Couette flow, the non-linear Fourier flow between parallel plates and the non-linear Poiseuille flow between parallel plates. The numerical results obtained using the developed PIC codes were compared to results found in the literature and analytical solutions at the free molecular limit. In all cases a very good agreement has been observed.

The accurate simulation of those three benchmark problems leads the way for the extension of the developed methodology. Some potential extensions include PIC codes for 2D or 3D flows as well as for axisymmetric flows. Another interesting extension could be to solve the exact Boltzmann equation, without using kinetic models and instead by estimating the collision integral using Monte Carlo integration.

References

- [1]: Bernoulli, Daniel. Hydrodynamica. 1738.
- [2]: Clausius, Rudolf. "On the Nature of the Motion which we call Heat." Philosophical Magazine (1875): 108-127.
- [3]: Maxwell, J.C. "Illustrations of the dynamical theory of gases." Philosophical Magazine (1860): 19, 19-32 and 20, 21-37.
- [4]: Boltzmann, L. "Weitere Studien über das Wärmegleichgewicht unter Gasmolekülen." Wiener Berichte (1872): 66, 275-370.
- [5]: Einstein, A. "Über die von der molekularkinetischen Theorie der Wärme geforderte Bewegung von in ruhenden Flüssigkeiten suspendierten Teilchen" Annale der Physik (1905), 17 (8), 549-560.
- [6]: Smoluchowski, M. "Zur kinetischen Theorie der Brownschen Molekularbewegung und der Suspensionen" Annalen der Physik (1906), 21 (14), 756-780.
- [7]: Aristov, V., Ilyin, O. "Kinetic models for historical processes of fast invasion and aggression" Phys. Rev. E (2015), 91, 042806.
- [8]: Shen, Ching. Rarefied Gas Dynamics, Fundamentals, Simulations and Micro Flows. 2005.
- [9]: Sone, Yoshio. Molecular Gas Dynamics, Theory, Techniques and Applications. 2007.
- [10]: Bird, G.A. Molecular Gas Dynamics. 1976.
- [11]: Cercignani, C. The Boltzmann equation and its Applications. 1988.
- [12]: Bhatnagar P.L., Gross E.P., Krook. M. "A model for Collision Processes in Gases. I. Small Amplitude Processes in Charged and Neutral One-Component Systems." Physical Review (1954): 94(3) 511-525.
- [13]: Shakhov, E.M. "Generalization of the Krook kinetic relaxation equation." Fluid Dyn. (1968): 3(5) 95-96.
- [14]: Holway, L.H. Approximation procedure for kinetic theory. PhD thesis, Harvard University, 1963.
- [15]: Rykov, V.A. "Model Kinetic Equations for a Gas with Rotational Degrees of Freedom." Izv. Akad. Nauk. SSSR. Mekh. Zhidk. Gaza. (1975): (6), 701-115.
- [16]: Holway, L.H. "New statistical models for kinetic theory." Physics of Fluids (1966): 9: 1658-1673.

- [17]: McCormack, F.J. "Construction of linearized kinetic models for gaseous mixtures and molecular gases." Physics of Fluids (1973): 16: 2095.
- [18]: Jaghargh, A. A., Roohi, E., Stefanov, S. "DSMC simulation of micro/nano flows using SBT-TAS technique" Computers & Fluids (2014), 102, 266-276.
- [19]: H. Struchtrup, P. Taheri. "Macroscopic transport models for rarefied gas flows: A brief review." IMA Journal of Applied Mathematics (76 (5) 672-697): 201
- [20]: Grigoryev, Yu. N., Vshivkov, V. A., Fedoruk, M. P. "Numerical particle-in-cell methods theory and applications" Utrecht, Boston (2002).
- [21]: Berezin. Yu. A., Vshivkov V.A., "Particle-in-cell method in rarefied plasma dynamics" (1980), Novosibirsk: Nauka.
- [22]: Babenko. K.I. "Theoretical foundation and construction of the numerical algorithms for the problems of mathematical physics" (1979), Moscow: Nauka.
- [23]: Yanenko. N.N., Anuchina. N.N., Petrenko V.E., Shokin. Yu.I. "On the calculation methods for gasdynamic problems with large deformations" Chislennyye metody mexaniki sploshnoi sredy. (1970), 1, 40-62.
- [24]: Belotserkovsky O.M., Davyudov. Yu.M. "A coarse particle method in gas dynamic" Moscow: Nauka (1982).
- [25]: Belotserkovsky. O.M., Yanitsky. V.E. "The statistical particle-in-cell method for solving rarefied gas dynamics problems" J. vychislitelnoi matematiki i matematicheskoi fiziki (1975), 15 (5), 1195-1208.
- [26]: Belotserkovsky. O.M. "Numerical modeling in the mechanics of continuous media" Moscow: Nauka (1984).
- [27]: H. A. Stone, A. D. Stroock, A. Ajdari. "Engineering flows in small devices: microfluidics towards a lab-on-chip." Annual Review of Fluid Mechanics 36 (2014): 381-411.
- [28]: H.A. Yang, M.C. Wu, W.L. Fang. "Localized induction heating solder bonding for wafer level MEMS packaging." Journal of Micromechanics and Microengineering (2005): 15, 394-399.
- [29]: H. Liu, M. Wang, J. Wang, G. Zhang, H. Liao, R. Huang, X. Zhang. "Monte Carlo simulations of gas flow and heat transfer in vacuum packaged MEMS devices." Applied Thermal Engineering (2007): 27: 323-329.
- [30]: Y. Sone, Y. Waniguchi, K. Aoki, S. Takata. "One-way flow of a rarefied gas induced in a channel with a periodic temperature distribution." Physics of Fluids (1996): 8(8), 2227-2235.

- [31]: A. Alexeenko, S. Gimelshein, E. Muntz, A. Ketsdever. “Kinetic modeling of temperature driven flows in short microchannels.” International Journal of Thermal Sciences (2006): 45, 1045-1051.
- [32]: A. Ketsdever, N. Gimelshein, S. Gimelshein, N. Selden. “Radiometric phenomena: From the 19th to the 21st century.” Vacuum (2012): 86, 1644-1662.
- [33]: M. Vargas, M. Wüest and S. Stefanov. “Monte Carlo analysis of thermal transpiration effects in capacitance diaphragm gauges with helicoidal baffle system.” Journal of Physics: Conference 362, 012013, 2012 (n.d.).
- [34]: Aoki. K., Takata. S., Nakanishi. T. “Poiseuille-type flow of a rarefied gas between two parallel plates driven by a uniform external force” Phys. Rev. E (2002), 65, 026315.
- [35]: Misdanitis. S., Valougeorgis. D. “Couette flow with heat transfer in the whole range of the Knudsen number” 6th International Conference on Nanochannels, Microchannels and Minichannels, June 23-25, 2008, Darmstadt, Germany, Paper No ICNMM2008-62079, Publisher: ASME.
- [36]: Pantazis, S. “Simulation of transport phenomena in conditions far from thermodynamic equilibrium via kinetic theory with applications in vacuum technology and MEMS” PhD thesis, University of Thessaly, 2011.